Alexandria Engineering Journal (2021) 60, 4067–4083

HOSTED BY

ELSEVIER

Alexandria University

Alexandria Engineering Journal

www.elsevier.com/locate/aej
www.sciencedirect.com

Interfacial layer and shape effects of modified Hamilton's Crosser model in entropy optimized Darcy-Forchheimer flow

M.K. Nayak [a], **S. Shaw** [b], **M. Ijaz Khan** [c], **O.D. Makinde** [d], **Yu-Ming Chu** [e,f,*], **Sami Ullah Khan** [g]

[a] *Department of Mechanical Engineering, ITER, Siksha 'O' Anusandhan Deemed to be University, Bhubaneswar, Oldisha, India*
[b] *Department of Mathematics and Statistical Sciences, Botswana International University of Science and Technology, Private Bag 16, Palapye, Botswana*
[c] *Department of Mathematics and Statistics, Riphah International University I-14, Islamabad 44000, Pakistan*
[d] *Faculty of Military Science, Stellenbosch University, Private Bag X2, Saldanha 7395, South Africa*
[e] *Department of Mathematics, Huzhou University, Huzhou 313000, PR China*
[f] *Hunan Provincial Key Laboratory of Mathematical Modeling and Analysis in Engineering, Changsha University of Science & Technology, Changsha 410114, PR China*
[g] *Department of Mathematics, COMSATS University Islamabad, Sahiwal 57000, Pakistan*

Received 15 October 2020; revised 28 January 2021; accepted 9 February 2021
Available online 12 March 2021

KEYWORDS

Darcy-Forchheimer flow;
Non linear thermal radiation;
Modified Hamilton's Crosser Model;
Porous irreversibility

Abstract In this analysis, the interfacial layer and shape effects has been inspected numerically for the Darcy Forchheimer electromagnetic flow of single-walled carbon nanotubes (SWCNT) and multi-walled carbon nanotubes (MWCNTs) with base fluid (water) nanofluids. The influence of nonlinear thermal radiation and homogenous and heterogeneous chemical reactions are also taken into account. A revised Hamilton Crosser model is implemented for measuring interfacial layer and shape effects of carbon nanotubes-water nanofluid. The flow problem for examining the heat transfer features has been modeled in term of nonlinear equations by incorporating the Hamilton–Crosser model. The main objective for performing the current work is to analyze how the shapes of nanoparticles effect towards the flow of considered fluid with various thermal features. The entropy generation analysis is performed as novelty. The governing dimensionless equations are numerically solved by fourth order Runge–Kutta method computational shooting technique. The relevant parameter variations on axial, radial, tangential velocity, temperature, concentration, skin friction, Nusselt number, entropy generation rate and Bejan number are highlighted. The enhanced shape factor of nanoparticles contributes to accelerated flow along axial and radial directions while it yields decelerated flow along tangential direction of lower and upper disks. The

* Corresponding author at: Department of Mathematics, Huzhou University, Huzhou 313000, PR China.
E-mail address: chuyuming@zjhu.edu.cn (Y.-M. Chu).

Peer review under responsibility of Faculty of Engineering, Alexandria University.

https://doi.org/10.1016/j.aej.2021.02.010

Nomenclature

(u, v, w)	velocity components in increasing (r, ϕ, z) directions $\left(m\,s^{-1}\right)$
nf	nanofluid
np	nanoparticle
bf	basefluid
HT	heat transfer
HTR	heat transfer rate
NLTR	non linear thermal radiation
HHR	homogeneous and heterogeneous reactions
SVD	surface viscous drag
CNT	carbon nanotube
SWCNT	single walled CNT
MWCNT	multiwalled CNT
LD	lower disk
UD	upper disk
BLT	boundary layer thickness
TBLT	thermal boundary layer thickness
TC	thermal conductivity
HC	heat capacitance
EDV	effective dynamic viscosity
TE	thermal expansion
ρ_{nf}	effective density of the nf $\left(kg\,m^{-3}\right)$
ρ_s	density of CNTs $\left(kg\,m^{-3}\right)$
ρ_f	density of bf $\left(kg\,m^{-3}\right)$
$\left(\rho C_p\right)_{nf}$	HC of the nf $\left(J\,kg^2\,m^3 K^{-1}\right)$
$\left(\rho C_p\right)_f$	HC of bf $\left(J\,kg^2\,m^3 K^{-1}\right)$
$\left(\rho C_p\right)_{CNT}$	HC of CNTs $\left(J\,kg^2\,m^3 K^{-1}\right)$
μ_{nf}	EVD of the nf $\left(kg\,m^{-1} s^{-1}\right)$
μ_f	EVD of bf $\left(kg\,m^{-1} s^{-1}\right)$
β_f	TE of bf $\left(K^{-1}\right)$
β_s	TE of CNTs $\left(K^{-1}\right)$
k_{nf}	TC of nf $\left(W\,m^{-1}\,K^{-1}\right)$
k_f	TC of bf $\left(W\,m^{-1}\,K^{-1}\right)$
k_s	TC of CNTs $\left(W\,m^{-1}\,K^{-1}\right)$
p	pressure (Pa)
T	fluid temperature in the boundary layer (K)
(T_1, T_2)	temperatures of (LD,UD) (K)
(C_1, C_2)	concentrations of species A and B $(moles/litre)$
$\sigma*$	Stefan Boltzmann constant
$k*$	mean absorption coefficient
C_0	ambient concentration $(moles/litre)$
B_0	uniform strength of magnetic field $(Tesla)$
E_0	uniform strength of electric field (V/m)
K	porous medium permeability
$F\left(=\frac{c_d}{\sqrt{K^*}}\right)$	inertia coefficient in the porous medium
c_d	drag coefficient
(h_1, h_2)	convective heat transfer coefficients at (LD, UD) $\left(Wm^{-2}K^{-1}\right)$
ϕ	solid volume fraction
Re	rotational Reynolds number
G_r	thermal Grashof number
M	Hartman number
(A_1, A_2)	stretching parameters for (LD, UD)
Ω	rotation parameter
Pr	Prandtl number
Sc	Schmidt number
Nr	radiation parameter
K_1	homogeneous reaction parameter
K_2	heterogeneous reaction parameter
E_c	Eckert number
θ_r	temperature ratio parameter
(B_1, B_2)	Biot numbers
P	porosity parameter
E_1	electric field parameter
F_r	local inertia coefficient
Br	Brinkman number
α	temperature difference parameter
(β_1, β_2)	diffusion parameters with respect to (homogeneous, heterogeneous) reaction

Subscripts

nf	nanofluid
f	base fluid
CNT	carbon nanotube

augmented interfacial layer parameter enhances heat transportation from the surfaces of lower and upper disks.

1. Introduction

Due to remarkable thermal performances of nano-materials, the scientists have intended some special attention on this topic in recent decade. The nanoparticles attain enhanced thermal properties as compared to the normal fluids. The conventional base materials like biological liquids, water, oil, ethylene glycol offer less thermal performances which report poor conductivity process. The thermal transport of nano-materials evaluate novel applications in solar energy, nuclear reactor, space technology, cooling devices, microelectronics, bio-medical applications, treatment of diseases, cancer tissues etc. The shape and size of such nano-metallic particles attribute the thermal assessment of nanofluids [1–7].

Nanolayer is the solid-like structure developed in between the surface of base fluid molecules and nanoparticles [8]. In fact, interfacial layer in nanoparticles is a nano-scaled shell surrounding the particles. It comprises of liquid molecules but behaves as solids. Because the interfacial layer is placed at the liquid-solid interface, it plays a role like an intermediate physical state with complex interface electrostatic effects and therefore acts as an important thermal bridge between the nanoparticles and base fluid. The thickness of this interfacial liquid layer is of the order of nanometer. Such nanolayer plays a vital role in heat transportation from solid to the adjacent liquid.

In the history of progress of nanotechnology in the twenty-first century, carbon nanotubes (CNTs) such as single-walled carbon nanotubes (SWCNT) and multi-walled carbon nanotubes (MWCNTs) possessing outstanding electrical, thermal, mechanical, chemical and optical properties are being considered as prime candidate materials in multidisciplinary fields including material science, automotive, optical, electrical, aerospace, bio-medical and energy conversion for nano-scale applications [9,10]. Experimental and theoretical studies have ensured that thermal conductivity of cylindrical structured nanoparticles is higher than that of spherical nanoparticles [9]. In view of high thermal conductivity, large specific surface area (SSA), high aspect ratio and low specific gravity, carbon nanotubes have been chosen by researchers as best suitable nanoparticles to improve the overall thermal conductivity and therefore the performance of existing heat transfer system. Choi et al. [11] successfully presented the basic work on thermal aspects of nanoparticles. In their pioneering study they dispersed multi-walled carbon nanotubes nanoparticles in synthetic poly oil base fluid. They found 160% augmentation in thermal conductivity for 1.0 vol% of carbon nanotubes nanoparticles. Henceforward, many researchers studied on the flow and heat transfer of nanofluids with consideration of different base fluids and carbon nanotubes as nanoparticles subject to different geometries in varied homogeneous/heterogeneous media. Nadeem and Shehzadi [12] examined the heat transfer features in the peristaltic transport of viscous fluid by using single wall carbon nanotube. Mahanthesh et al. [13] examined the applications of irregular heat source in flow of both single and multi-walled wall carbon nanotubes confined by rotating disks. The impact of homogeneous and heterogeneous chemical reactions in flow of single-walled carbon nanotubes over plane surface has been analyzed numerically by Ahmed et al. [14]. Chaudhary and Kanika [15] studied the marangoni convection flow of single-walled carbon nanotubes (SWCNT) and multi-walled carbon nanotubes (MWCNTs) in presence of magnetic force. The experimental analysis for flow of hybrid nanofluid was inspected by Shahsavar and Bahiraei [16]. Shehzad et al. [17] analyzed the thermal enhancement of single-walled carbon nanotubes and multi-walled carbon nanotubes in presence of slip effects and exponential heat source. Dawar et al. [18] discussed the unsteady squeezing flow of carbon nanotube induced by rotating channels along with external features of entropy generation and viscous dissipations.

Entropy generation minimization (EGM) is inevitable in all real life and practical applications, for example, heat pumps, power plants, air conditioners, heat engines and refrigerators etc undergoing flow and heat transportation with objective of enhancement of thermal efficiency. Bejan [19] was the first researcher who disclosed the fundamental causes of entropy generation in the convective heat transfer problems. Many researchers (Farooq et al. [20], Nayak et al. [21], Khan et al. [22], Chamkha et al. [23], Afridi et al. [24], Khan et al. [25], Khan et al. [26]) then investigated the EG analysis and the effect of entropy generation minimization in the various flow problems.

Motivated in a thoughtful essay on the literature survey, we have studied the influence of interfacial nanolayer and shape effect in the electromagnetic flow of SWCNT/MWCNT-water nanofluids subject to homogenous and heterogeneous chemical reactions and nonlinear thermal radiation. The applications of porous medium have been suggestion by using Darcy Forchheimer relations [27–29].

Based on authors' knowledge and above literature survey it is obvious that the problem of interfacial nanolayer effect subject to two rotating disks is not investigated in earlier works. The effective thermal properties of nanoparticles are studied by using the modified Hamilton and Crosser model. This modified model was originally introduced by Hamilton and Crosser in 1962 [30]. Based on this model, the suggested expressions convey applications of nanoparticles size, shape in addition to the volume fraction. The inspection of nanoparticles shape, size and various thermal mechanisms can be effectively predicted by incorporating Hamilton and Crosser model. Based on Hamilton and Crosser mdel, many interesting contributions have been suggested by scientists [31–37]. The motivating objective of this analysis is to inspect how the shapes of nanoparticles effect towards the flow of considered fluid with various thermal features. Runge–Kutta method of fourth order is the novel numerical approach for the developed non dimensional equations of the present problem. The distinguished characteristics of axial, radial and tangential velocity, temperature and nanoparticles concentration, Nusselt number, entropy generation and Bejan numbers under the influence of interfacial nanolayer and shape factor in presence of NLTR and HHRs are explored with aid of suitable graphs and extended numerical tables.

2. Physical model

We consider a steady Darcy-Forchheimer electromagnetic flow of nanofluid with SWCNT and MWCNT suspensions between two stretchable parallel rotating disks subject to subject to nonlinear thermal radiation and homogenous and heterogeneous chemical reactions. An incompressible viscous fluid saturates the porous space describing Darcy-Forchheimer expression. In this study, pure water is considered as base fluid and single-walled carbon nanotubes (SWCNT) and multi-walled carbon nanotubes (MWCNTs) is taken as nanoparticles. Both disks rotate with angular velocities (Ω_1 and Ω_2) and stretching rates (a_1 and a_2) respectively. We assume that the bottom surface of the disk gets heated by convection from a hot fluid with temperature T_0 while that of upper disk as T_1. The disks are h distant apart as shown in Fig. 1.

The homogenous reaction in cubic autocatalysis is defined as:

$A + 2B \rightarrow 3B$, rate $= k_c C_1 C_2^2$

The expressions for first order isothermal reaction on the catalyst surface are:

$A \rightarrow B$, rate$= k_s C_1$where k_c and k_s represents the rate constants while C_1 and C_2 denote the concentration of chemical species A and B, respectively. It is assumed that reaction rate is minor in the outer edge of boundary and in the external flow regime. Further, it is assumed that both reaction processes are isothermal.

The governing physical equations are [5–7]:

$$\frac{\partial u}{\partial r} + \frac{u}{r} + \frac{\partial w}{\partial z} = 0, \tag{1}$$

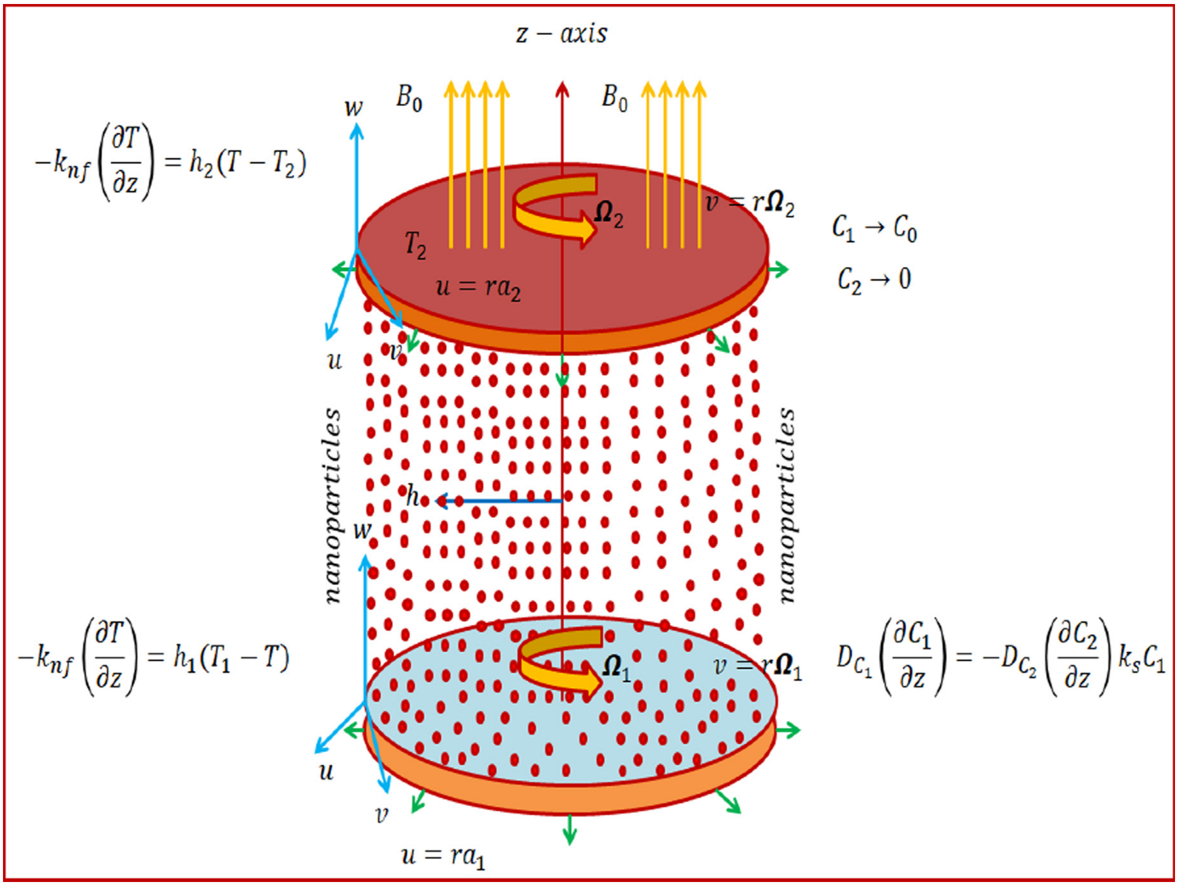

Fig. 1 Flow model.

$$u\frac{\partial u}{\partial r} - \frac{v^2}{r} + w\frac{\partial u}{\partial z} = -\frac{1}{\rho_{nf}}\frac{\partial p}{\partial r} + \frac{\mu_{nf}}{\rho_{nf}}\left(\frac{\partial^2 u}{\partial r^2} + \frac{1}{r}\frac{\partial u}{\partial r} - \frac{u}{r^2} + \frac{\partial^2 u}{\partial z^2}\right) + \frac{(\rho\beta)_{nf}}{\rho_{nf}}g(T - T_2) + \frac{\sigma_{nf}}{\rho_{nf}}\left(E_0B_0 - B_0^2 u\right) - \frac{\mu_{nf}}{\rho_{nf}}\frac{u}{K} - Fu^2, \quad (2)$$

$$u\frac{\partial v}{\partial r} + \frac{uv}{r} + w\frac{\partial v}{\partial z} = \frac{\mu_{nf}}{\rho_{nf}}\left(\frac{\partial^2 v}{\partial r^2} + \frac{1}{r}\frac{\partial v}{\partial r} - \frac{v}{r^2} + \frac{\partial^2 v}{\partial z^2}\right) + \frac{(\rho\beta)_{nf}}{\rho_{nf}}g(T - T_2) + \frac{\sigma_{nf}}{\rho_{nf}}\left(E_0B_0 - B_0^2 v\right) - \frac{\mu_{nf}}{\rho_{nf}}\frac{v}{K} - Fv^2, \quad (3)$$

$$u\frac{\partial w}{\partial r} + w\frac{\partial w}{\partial z} = -\frac{1}{\rho_{nf}}\frac{\partial p}{\partial z} + \frac{\mu_{nf}}{\rho_{nf}}\left(\frac{\partial^2 w}{\partial r^2} + \frac{1}{r}\frac{\partial w}{\partial r} + \frac{\partial^2 w}{\partial z^2}\right), \quad (4)$$

$$(\rho C_p)_{nf}\left(u\frac{\partial T}{\partial r} + w\frac{\partial T}{\partial z}\right) = \left(k_{nf} + \frac{16\sigma^* T^3}{3k^*}\right)\left(\frac{\partial^2 T}{\partial r^2} + \frac{1}{r}\frac{\partial T}{\partial r} + \frac{\partial^2 T}{\partial z^2}\right) + \left(\frac{16\sigma^* T^2}{k^*}\right)\left(\left(\frac{\partial T}{\partial r}\right)^2 + \left(\frac{\partial T}{\partial z}\right)^2\right) + \mu_{nf}\left[\left(\frac{\partial u}{\partial z}\right)^2 + \left(\frac{\partial v}{\partial z}\right)^2\right] + \sigma_{nf}\left[(u^2 + v^2)B_0^2 - 2E_0^2\right] + \frac{\mu_{nf}(u^2+v^2)}{K} + \rho_{nf}F(u^3 + v^3), \quad (5)$$

$$u\frac{\partial C_1}{\partial r} + w\frac{\partial C_1}{\partial z} = D_{C_1}\left(\frac{\partial^2 C_1}{\partial r^2} + \frac{1}{r}\frac{\partial C_1}{\partial r} + \frac{\partial^2 C_1}{\partial z^2}\right) - k_c C_1 C_2^2, \quad (6)$$

$$u\frac{\partial C_2}{\partial r} + w\frac{\partial C_2}{\partial z} = D_{C_2}\left(\frac{\partial^2 C_2}{\partial r^2} + \frac{1}{r}\frac{\partial C_2}{\partial r} + \frac{\partial^2 C_2}{\partial z^2}\right) + k_c C_1 C_2^2, \quad (7)$$

with

$$\left.\begin{array}{c} u = ra_1,\ v = r\Omega_1,\ w = 0, -k_{nf}\left(\frac{\partial T}{\partial z}\right) = h_1(T_1 - T), \\ D_{C_1}\left(\frac{\partial C_1}{\partial z}\right) = -D_{C_2}\left(\frac{\partial C_2}{\partial z}\right) = k_s C_1 \ at\ z = 0 \\ u = ra_2,\ v = r\Omega_2,\ w = 0, \\ -k_{nf}\left(\frac{\partial T}{\partial z}\right) = h_2(T - T_2),\ C_1 \to C_0,\ C_2 \to 0 \quad as\ z \to h \end{array}\right\} \quad (8)$$

In ABOVE boundary conditions, $u = ra_1$ and $u = ra_2$ are the radial boundary conditions. Here "u" the radial velocity while a_1 and a_2 are the stretching rates. It is remarked that a_1 is the lower disk stretching rate along the radial direction while a_2 is the upper disk stretching rate along the radial direction.

The physical, thermal and electrical properties of nanofluid are:

$$\left.\begin{array}{c} \mu_{nf} = \frac{\mu_f}{(1-\phi)^{2.5}}, \\ \rho_{nf} = (1-\phi)\rho_f + \phi\rho_{CNT}, \\ (\rho C_p)_{nf} = (1-\phi)(\rho C_p)_f + \phi(\rho C_p)_{CNT}, \\ (\rho\beta)_{nf} = (1-\phi)(\rho\beta)_f + \phi(\rho\beta)_{CNT}, \\ \sigma_{nf} = \sigma_f\left[1 + \frac{3\left(\frac{\sigma_{CNT}}{\sigma_f} - 1\right)\phi}{\left(\frac{\sigma_{CNT}}{\sigma_f} + 2\right) - \left(\frac{\sigma_{CNT}}{\sigma_f} - 1\right)\phi}\right] \end{array}\right\} \quad (9)$$

Jiang et al. [8] developed a renovated Hamilton-Crosser model in order to introduce the effect of the interfacial nanolayer as well as an empirical shape factor in effective thermal conductivity of carbon nanotube (CNT) based nanofluid within the parameter range $0 \leqslant \phi \leqslant 0.01$. In this case, mono-sized ellipsoidal particles having semi-axes a, b, and c ($a \geqslant b \geqslant c$) are covered by interfacial nanolayer around them (see Fig. 2).

The nanolayer possesses an intermediate thermal conductivity between the base liquid, k_f and the CNT, k_p because the layered molecules exist in an intermediate physical state between a liquid and a solid. Hence, Jiang et al. [8] revised the Hamilton and Crosser model [30] and developed new model depicting effective thermal conductivity as

$$k_{nf} = k_f \frac{k_{pe} + (n-1)k_f + (n-1)\left(k_{pe} - k_f\right)\phi_e}{k_{pe} + (n-1)k_f - \left(k_{pe} - k_f\right)\phi_e}, \quad (10)$$

where k_{pe} is the thermal conductivity of the equivalent nanoparticles (nanoparticles/nanolayer composite), ϕ_e is the effective nanoparticles volume fraction and n is an empirical shape factor, k_l is the average thermal conductivity of the interfacial nanolayer.

Here,

$$k_{pe} = \frac{2k_p + \left[\left(1+\frac{t}{b}\right)^2 - 1\right]\left(k_p + k_l\right)}{2k_l + \left[\left(1+\frac{t}{b}\right)^2 - 1\right]\left(k_p + k_l\right)} k_l, \quad (11)$$

$$\phi_e = \left(1 + \frac{t}{b}\right)^2 \phi, \quad (12)$$

$$n = sph^{-\gamma}, \quad (13)$$

$$k_l = k_f \frac{1 + \frac{t}{b} - a}{a\frac{t}{b}} \frac{\ln\left(1+\frac{t}{b}\right)}{\ln\left(\frac{1+\frac{t}{b}}{a}\right)} \quad (14)$$

(for cylindrical particle with $a \geqslant b = c$)

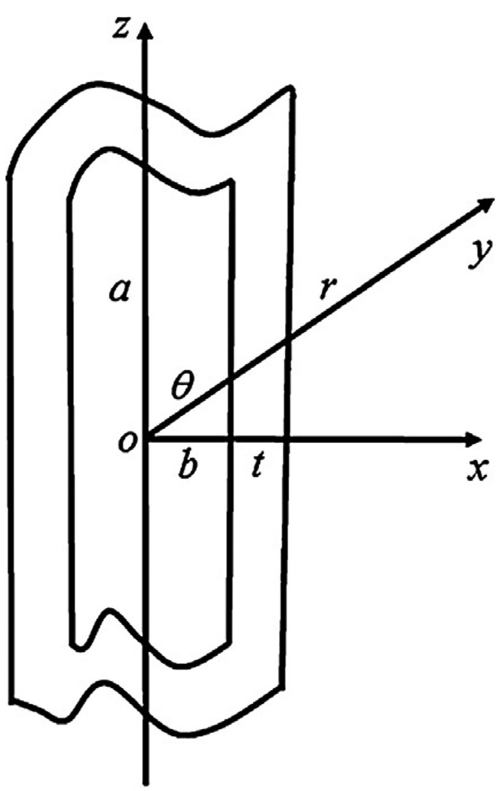

Fig. 2 Schematic of the cylindrical nanoparticles with an interfacial nanolayer.

The sphericity, for a cylindrical particle [35]:

$$sph = \frac{2e(\delta)\left[1 - e^2(\delta)\right]^{\frac{1}{6}}}{e(\delta)\sqrt{1 - e^2(\delta)} + arc\,Sine(\delta)}, \quad (15)$$

with e as the eccentricity of the nanoparticles and δ lying between 0 and t.

The transformations include:

$$\left.\begin{array}{c} (u, v, w) = \left(r\Omega_1 f'(\zeta),\ r\Omega_1 g(\zeta),\ -2h\,\Omega_1 f(\zeta)\right), \\ \theta(\zeta) = \frac{T - T_2}{T_1 - T_2},\ p = \rho_f \Omega_1 \upsilon_f \left\{P(\zeta) + \frac{1}{2}\frac{r^2}{h^2}\varepsilon\right\}, \\ \phi(\zeta) = \frac{C_1}{C_0}, \chi(\zeta) = \frac{C_2}{C_0},\ \zeta = \frac{z}{h}. \end{array}\right\} \quad (16)$$

where ε is the pressure parameter, η is the non-dimensional distance along the axis of rotation. Further, f, g and θ are functions of η. From (12),

$$\theta(\zeta) = \frac{T - T_2}{T_1 - T_2},$$

$$\text{Or } T = T_2\left[1 + (\theta_r - 1)\theta\right], \quad (17)$$

where $\theta_r = \frac{T_1}{T_2}$ is the temperature ratio parameter.

Taking help of (9) to (17), (2) to (8) take the form

$$\Gamma_2 f''' + Re\left[2ff'' - (f')^2 + g^2\right] + \frac{Gr}{Re}\Gamma_3\theta + \Gamma_1\Gamma_4 MRe(E_1 - f') - PRe\Gamma_2 f' - F_r Re(f')^2 - \varepsilon\Gamma_1 = 0, \quad (18)$$

$$\Gamma_2 g'' + 2Re(fg' - gf') + \frac{Gr}{Re}\Gamma_3\theta + \Gamma_1\Gamma_4 MRe(E_1 - g) - PRe\Gamma_2 g - F_r Reg = 0, \quad (19)$$

$$\Gamma_1 P' + 4Reff' + 2\Gamma_2 f'' = 0, \quad (20)$$

$$\Gamma_5\left\{\left(\Gamma_6 + \tfrac{4}{3Nr}\left[1 + (\theta_r - 1)\theta\right]^3\right)\theta'' + \tfrac{4}{Nr}\left[1 + (\theta_r - 1)\theta\right]^2(\theta_r - 1)(\theta')^2\right\} + 2\Pr Ref\theta' + \Gamma_7 Br\left[(f'')^2 + g^2\right] + \Gamma_4\Gamma_5 M\,Re\,Br\left[(f')^2 + g^2 - 2E_1^2\right] + \tfrac{\Gamma_5}{\Gamma_1} BrReFr\left[(f')^3 + g^3\right] = 0, \quad (21)$$

$$\frac{1}{Re\,Sc}\phi'' + 2f\phi' - K_1\phi\chi^2 = 0, \quad (22)$$

$$\delta\frac{1}{Re\,Sc}\chi'' + 2f\chi' + K_1\phi\chi^2 = 0, \quad (23)$$

$$\left.\begin{array}{c} f(0) = 0, f'(0) = A_1,\ g(0) = 1, \\ \Gamma_5\theta'(0) = -B_1[1 - \theta(0)],\ \phi'(0) = -\delta\chi'(0) = K_2\phi(0), \\ f(1) = 0, f'(1) = A_2,\ g(1) = \Omega, \\ \Gamma_5\theta'(1) = -B_2[1 - \theta(1)],\ \phi(1) = 1,\ \chi(1) = 0,\ P(0) = 0. \end{array}\right\} \quad (24)$$

We assume that D_{C_1} and D_{C_2} are equal, i.e., $\Omega = 1$. This assumptions develops the relation

$$\phi(\zeta) + \chi(\zeta) = 1, \quad (25)$$

Using (25), (22) and (24) become

$$\frac{1}{Re\,Sc}\phi'' + 2f\phi' - K_1\phi(1 - \phi)^2 = 0, \quad (26)$$

$$\left.\begin{aligned} & f(0)=0, f'(0)=A_1, g(0)=1, \\ & \Gamma_5\theta'(0)=-B_1[1-\theta(0)],\ \phi'(0)=K_2\phi(0), \\ & f(1)=0, f'(1)=A_2, g(1)=\Omega, \\ & \Gamma_5\theta'(1)=-B_2[1-\theta(1)],\ \phi(1)=1,\ P(0)=0. \end{aligned}\right\} \tag{27}$$

Differentiating (18) with respect to ζ,

$$\Gamma_2 f^{iv}+Re[2ff'''+2gg']+\frac{Gr}{Re}\Gamma_3\theta' - (\Gamma_1\Gamma_4 MRe+PRe\Gamma_2)f''-2F_rReff''=0, \tag{28}$$

The pressure term can be obtained by integrating (20) with respect to ζ and taking limit from 0 to ζ.

We have,

$$\Gamma_1 P+2\{Ref^2+\Gamma_2[f'-f'(0)]\}=0, \tag{29}$$

In the aforesaid equations, we have

$$\left.\begin{aligned} & Re=\tfrac{r\Omega_1 h}{\upsilon_f},\ Gr=\tfrac{g\beta_f T_2(\theta_r-1)h^3}{\upsilon_f^2},\ M=\tfrac{\sigma B_0^2 h}{r\Omega_1}, A_1=\tfrac{a_1}{\Omega_1}, \\ & A_2=\tfrac{a_2}{\Omega_1},\ \Omega=\tfrac{\Omega_2}{\Omega_1},\ E_1=\tfrac{E_0}{B_0 r\Omega_1},\ P=\tfrac{\upsilon_f h}{Kr\Omega_1},\ F_r=Fh,\ \theta_r=\tfrac{T_1}{T_2}, \\ & \Pr=\tfrac{\upsilon_f}{\alpha_f},\ Nr=\tfrac{k^*k_f}{4\sigma^* T_2^3},\ E_c=\tfrac{r^2\Omega_1^2}{T_2(\theta_r-1)(c_p)_f},\ Br=\Pr.E_c, \\ & Sc=\tfrac{\upsilon_f}{D_{c_1}},\ K_1=\tfrac{k_0 C_0^2}{\Omega_1},\ K_2=\tfrac{k_s h}{D_{c_1}},\ B_1=\tfrac{hh_1}{k_f}, B_2=\tfrac{hh_2}{k_f} \end{aligned}\right\} \tag{30}$$

and

$$\left.\begin{aligned} & \Gamma_1=\frac{1}{(1-\phi)+\phi\left(\frac{\rho_{CNT}}{\rho_f}\right)},\ \Gamma_2=\frac{1}{(1-\phi)^{2.5}\left\{(1-\phi)+\phi\left(\frac{\rho_{CNT}}{\rho_f}\right)\right\}}, \\ & \Gamma_3=\frac{(1-\phi)+\phi\left\{\frac{(\rho\beta)_{CNT}}{(\rho\beta)_f}\right\}}{(1-\phi)+\phi\left(\frac{\rho_{CNT}}{\rho_f}\right)},\ \Gamma_4=\frac{\sigma_{nf}}{\sigma_f},\ \Gamma_5=\frac{1}{(1-\phi)+\phi\left\{\frac{(\rho C_p)_{CNT}}{(\rho C_p)_f}\right\}}, \\ & \Gamma_6=\frac{k_{nf}}{k_f},\quad \Gamma_7=\frac{1}{(1-\phi)^{2.5}\left[(1-\phi)+\phi\left\{\frac{(\rho C_p)_{CNT}}{(\rho C_p)_f}\right\}\right]}. \end{aligned}\right\} \tag{31}$$

The surface drags at lower and upper disks (C_{f_1} and C_{f_2}) are $C_{f_1}=\frac{\tau_w|_{z=0}}{\rho_f(r\Omega_1)^2}$ and $C_{f_2}=\frac{\tau_w|_{z=h}}{\rho_f(r\Omega_1)^2}$,

Where shear stresses are defined as

$\tau_{zr}=\mu_{nf}\frac{\partial u}{\partial z}\Big|_{z=0}=\frac{\mu_f r\Omega_1 f''(0)}{h(1-\phi)^{2.5}}$ and $\tau_{z\theta}=\mu_{nf}\frac{\partial u}{\partial z}\Big|_{z=0}=\frac{\mu_f r\Omega_1 g'(0)}{h(1-\phi)^{2.5}}$,

Hence, the total shear stress is

$$\tau_w=\sqrt{\tau_{zr}^2+\tau_{z\theta}^2}=\frac{\mu_f r\Omega_1}{h(1-\phi)^{2.5}}\left\{[f''(0)]^2+[G'(0)]^2\right\}, \tag{32}$$

The non-dimensional surface drag forces become

$$C_{f_1}Re_r=\frac{1}{(1-\phi)^{2.5}}\left\{[F''(0)]^2+[G'(0)]^2\right\}^{\frac{1}{2}}, \tag{33}$$

$$C_{f_2}Re_r=\frac{1}{(1-\phi)^{2.5}}\left\{[F''(1)]^2+[G'(1)]^2\right\}^{\frac{1}{2}}, \tag{34}$$

The heat transfer rates for lower and upper disks (Nu_{r_1} and Nu_{r_2}) respectively are

$Nu_{r_1}=\frac{hq_w}{k_f(T_1-T_2)}\Big|_{z=0}$ and $Nu_{r_2}=\frac{hq_w}{k_f(T_1-T_2)}\Big|_{z=h}$,

Where the heat flux q_w reads

$q_w=-k_{nf}\left(\frac{\partial T}{\partial z}\right)+q_r|_{z=0}$ and $q_w=-k_{nf}\left(\frac{\partial T}{\partial z}\right)+q_r|_{z=h}$,

The non-dimensional local Nusselt numbers read

$$Nu_{r_1}=-\left[\Gamma_6+\frac{3}{4Nr}\{1+(\theta_r-1)\theta(0)\}^3\right]\theta'(0). \tag{35}$$

$$Nu_{r_2}=-\left[\Gamma_6+\frac{3}{4Nr}\{1+(\theta_r-1)\theta(1)\}^3\right]\theta'(1). \tag{36}$$

where $Re_r=\frac{r\Omega_1 h}{\nu_f}$ is the local Reynolds number.

3. Entropy generation analysis

The local entropy generation of the nanofluids is given by

$$\begin{aligned} S_G={}& \underbrace{\frac{k_f}{T_2^2}\left[\left(\frac{k_{nf}}{k_f}+\frac{16\sigma^*T^3}{3k_fk^*}\right)\left(\frac{\partial T}{\partial z}\right)^2\right]}_{\text{Thermal irreversibility}}+\underbrace{\frac{\mu_{nf}(u^2+v^2)}{T_2K}+\frac{\rho_{nf}F}{T_2}(u^3+v^3)}_{\text{Porous medium irreversibility}} \\ & em\underbrace{\frac{\mu_{nf}}{T_2}\left[\left(\frac{\partial u}{\partial z}\right)^2+\left(\frac{\partial v}{\partial z}\right)^2\right]}_{\text{Viscous dissipation irreversibility}}+\underbrace{\frac{\sigma_{nf}}{T_2}[(u^2+v^2)B_0^2-2E_0^2]}_{\text{Electromagnetic heating irreversibility}} \\ & +\underbrace{\frac{RD_{c_1}}{T_2}\left(\frac{\partial C_1}{\partial z}\right)\left(\frac{\partial T}{\partial z}\right)+\frac{RD_{c_1}}{C_1}\left(\frac{\partial C_1}{\partial z}\right)^2+\frac{RD_{c_2}}{T_2}\left(\frac{\partial C_2}{\partial z}\right)\left(\frac{\partial T}{\partial z}\right)+\frac{RD_{c_2}}{C_2}\left(\frac{\partial C_2}{\partial z}\right)^2}_{\text{Mass diffusion irreversibility of homogeneous and heterogeneous reactions}}, \end{aligned} \tag{37}$$

The entropy generation rate is

$$\begin{aligned} N_G={}&\alpha\left(\Gamma_6+\tfrac{4}{3Nr}\right)(\theta')^2+\tfrac{P}{(1-\phi)^{2.5}}\,Br\,Re\left[(f')^2+g^2\right] \\ &+\tfrac{FrReBr}{\phi_1}\left[(f')^3+g^3\right]+\tfrac{Br}{(1-\phi)^{2.5}}\left[(f'')^2+(g')^2\right] \\ &+\Gamma_4ReBrM\left[(f')^2+g^2-2E_1^2\right]+(\beta_1-\beta_2)\theta'\phi' \\ &+\tfrac{(\phi')^2}{\alpha}\left(\tfrac{\beta_1}{\phi}+\tfrac{\beta_2}{1-\phi}\right), \end{aligned} \tag{38}$$

The related Bejan number is

$$Be=\frac{\alpha\left(\Gamma_6+\frac{4}{3Nr}\right)(\theta')^2+(\beta_1-\beta_2)\theta'\phi'+\frac{(\phi')^2}{\alpha}\left(\frac{\beta_1}{\phi}+\frac{\beta_2}{1-\phi}\right)}{\begin{aligned}&\alpha\left(\Gamma_6+\tfrac{4}{3Nr}\right)(\theta')^2+\tfrac{P}{(1-\phi)^{2.5}}\,Br\,Re\left[(f')^2+g^2\right]+\tfrac{FrReBr}{\phi_1}\left[(f')^3+g^3\right]+\tfrac{Br}{(1-\phi)^{2.5}}\left[(f'')^2+(g')^2\right]\\&+\Gamma_4ReBrM\left[(f')^2+g^2-2E_1^2\right]+(\beta_1-\beta_2)\theta'\phi'+\tfrac{(\phi')^2}{\alpha}\left(\tfrac{\beta_1}{\phi}+\tfrac{\beta_2}{1-\phi}\right)\end{aligned}} \tag{39}$$

where $N_G=S_G\frac{h^2T_2}{k_f(T_1-T_2)}$ is the entropy generation rate, $Br=\frac{\mu_f r^2\Omega_1^2}{k_f(T_1-T_2)}$, $\alpha=\frac{T_1-T_2}{T_2}$ $\beta_1=\frac{RD_{C_1}C_0}{k_f}$, $\beta_2=\frac{RD_{C_2}C_0}{k_f}$.

4. Numerical solution

The system of governing equations (9), (15) and (16) are highly coupled and nonlinear. The analytical solution is not possible and hence, the numerical simulation is required to solve the governing equations with help of the given boundary condition (equation 17). The coupled and nonlinear governing equations are solved using shooting method of the symbolic computer algebraic software MATLAB by converting the boundary value problem into an initial value problem (IVP). At the initial stage, the higher order term of the differential equation is written in the lower order form as:

$$f^{iv} = -\frac{1}{\Gamma_2}\left[2Re(ff''' + gg') + \frac{Gr}{Re}\Gamma_3\theta' - \Gamma_1\Gamma_4 MRef'' + 2\frac{\Gamma_2 Re}{\Gamma_1}\left(Ref^2 + \Gamma_2(f' - A_1)\right)f'' - 2F_r Reff''\right], \quad (40)$$

$$g'' = -\frac{1}{\Gamma_2}\left[2Re(fg' - f'g) + \frac{Gr}{Re}\Gamma_3\theta' - \Gamma_1\Gamma_4 MRef'' + 2\frac{\Gamma_2 Re}{\Gamma_1}\left(Ref^2 + \Gamma_2(f' - A_1)\right)f'' - 2F_r Reff''\right], \quad (41)$$

$$\theta'' = -\frac{\frac{4\Gamma_5}{Nr}\{1 + (\theta_r - 1)\theta\}^2(\theta_r - 1)\theta'^2 + 2PrRef\theta'^2 + \Gamma_7 Br\left(f''^2 + g^2\right)@ + \Gamma_4\Gamma_5 MReBr\left(f^2 + g^2 - 2E_1^2\right) + \frac{\Gamma_5}{\Gamma_1}BrReF_r\left(f^3 + g^3\right)}{\Gamma_5\left[\Gamma_6 + \frac{4}{3N_R}\left(1 + (\theta_f - 1)\theta\right)^3\right]}, \quad (42)$$

$$\phi'' = -\mathrm{Re}Sc\left[2f\phi' - K\phi(1-\phi)^2\right]. \quad (43)$$

At the first, reduce the governing equations into a system of first order differential equations and for that introducing the new variables as:

$$y_1 = f,\ y_2 = f',\ y_3 = f'',\ y_4 = f''',\ y_5 = g,\ y_6 = g',\ y_7 = \theta, y_8 = \theta', y_9 = \phi, y_10 = \phi'. \quad (44)$$

Further, write the governing equations in a matrix form with $y = [f,\ f',f'',\ f''',\ g,\ g',\ \theta,\ \theta',\ \phi,\ \phi']^T$ as

$$\frac{d}{d\eta}\begin{pmatrix} y_1\\ y_2\\ y_3\\ y_4\\ y_5\\ y_6\\ y_7\\ y_8\\ y_9\\ y_{10}\end{pmatrix} = \begin{pmatrix} y_2\\ y_3\\ y_4\\ -\frac{1}{\Gamma_2}\left[2Re(y_1y_4 + y_5y_6) + \frac{Gr}{Re}\Gamma_3 y_8 - \Gamma_1\Gamma_4 MRey_3 + 2\frac{\Gamma_2 Re}{\Gamma_1}\left(Rey_1{}^2 + \Gamma_2(y_2 - A_1)\right)y_3 - 2F_r Rey_1y_3\right]\\ y_6\\ -\frac{1}{\Gamma_2}\left[2Re(y_1y_6 - y_2y_5) + \frac{Gr}{Re}\Gamma_3 y_8 - \Gamma_1\Gamma_4 MRey_3 + 2\frac{\Gamma_2 Re}{\Gamma_1}\left(Rey_1^2 + \Gamma_2(y_2 - A_1)\right)y_3 - 2F_r Rey_1y_3\right]\\ y_8\\ -\frac{\frac{4\Gamma_5}{Nr}\{1 + (\theta_r - 1)y_7\}^2(\theta_r - 1)y_8^2 + 2\mathrm{Pr}Rey_1y_8^2 + \Gamma_7 Br\left(y_3^2 + y_5^2\right) + \Gamma_4\Gamma_5 MReBr\left(y_2^2 + y_5^2 - 2E_1^2\right) + \frac{\Gamma_5}{\Gamma_1}BrReF_r\left(y_2^3 + y_5^3\right)}{\Gamma_5\left[\Gamma_6 + \frac{4}{3N_R}\left(1 + (\theta_f - 1)\theta\right)^3\right]}\\ \phi'\\ -ReSc\left[2y_1y_{10} - Ky_9(1 - y_9)^2\right]\end{pmatrix}, \quad (45)$$

and the corresponding boundary conditions can be written as

$$\begin{array}{ll} y_1(0),\ y_2(0) = A_1, & y_1(1) = 1,\ y_2(1) = A_2,\\ y_4(0) = 1, & y_5(1) = \Omega,\\ \Gamma_5 y_8(0) + B_1(1 - y_7(0)), & \Gamma_5 y_8(1) + B_2(1 - y_7(1)),\\ y_{10}(0) - K_2 y_9(0), & y_9(1), \end{array} \quad (46)$$

Secondly, we transform the given boundary value problem into an initial value problem and use an ordinary differential equations solver in MATLAB to numerically integrate this system, with the initial conditions given by

$$y(0) = \left[0,\ A_1,\ S_1,\ S_2,\ 1,\ S_3,\ S_4,\ -\frac{B_1}{\Gamma_5}(1 - S_4),\ S_5,\ K_2S_5\right], \quad (47)$$

where S_1, S_2, S_3, S_4 and S_5 are unknowns.

Thirdly, consider a guess value for the unknowns and solve equation (32) using the MATLAB's ODE solver. Shooting method is applied to find the initial guess which is based on the linear interpolation of the boundary value specified on the initial mesh of 15 equally spaced point is made. Continue the process until get a convergence and for that we bound the convergence criteria as error $|E_i| < \text{tolerance} = 10^{-10}$ where errors are defined as

$$\begin{aligned} E_1 &= y_3(\infty, S_1) - f''(\infty),\\ E_2 &= y_4(\infty, S_2) - f'''(\infty),\\ E_3 &= y_6(\infty, S_3) - g'(\infty),\\ E_4 &= y_7(\infty, S_4) - \theta(\infty),\\ E_5 &= y_9(\infty, S_5) - \phi(\infty), \end{aligned} \quad (48)$$

5. Results and discussion

In this section, a careful analysis on the characteristics of radial, axial and angular velocities, temperature and nanoparticles concentration, surface drag force (on the surface of lower and outer disks), HTR (from the surface of lower and outer disks), EG number and Bejan number under the influence of embedded physical parameters is carried on through the constructed apposite graphs and numerical tables. Such pertinent parameters include interfacial ratio parameter (t/b), particle volume fraction (ϕ), Reynolds number (Re), thermal Grashof number (Gr), Hartmann number (M), stretching parameter of lower disk A_1 and stretching parameter of upper disk A_2, rotation parameter (Ω), Prandtl number (Pr), Schmidt number (Sc), radiation parameter (Nr), homogeneous reaction parameter (K_1), heterogeneous reaction parameter (K_2), Eckert number (Ec), temperature ratio parameter (θ_r), thermal Biot numbers (B_1 and B_2), porosity parameter (P), electric field parameter (E_1), local inertia coefficient (F_r) and Brinkman number (Br), temperature difference parameter (α), diffusion parameter with respect to homogeneous reaction (β_1), diffusion parameter with respect to heterogeneous reaction (β_2). The fixed values of the embedded parameters include $Re = 0.1, Gr = 0.5, M = 1, F_r = 0.5, E_1 = 0.5, Nr = 0.2, \theta_r = 1.2,$ $Pr = 7, Br = 0.5, Sc = 20, K_1 = 0.2, K_2 = 0.1, A_1 = 0.5, A_2 = 0.1, \Omega = 0.5, B_1 = B_2 = 0.5, \phi = 0.01, \alpha = 0.1, \beta_1 = 0.1, \beta_2 = 0.2,$ $\phi_1 = 0.1$. Thermo physical properties of base fluid such as water and nanoparticle such as CNTs are incorporated in Table 1.

5.1. Axial velocity characteristics

This section imparts an embodiment of the axial velocity characteristics influenced by the significant physical parameters in

Table 1 Thermo-physical properties of the base fluid and nanoparticles at T = 300 K.

	$\rho(Kg/m^3)$	$C_P(J/KgK)$	$k(W/mK)$	$\mu_f(Ns/m^2)$
Pure Water	997.1	4179	0.613	0.001003
SWCNTs	2600	425	6600	
MWCNTs	1600	796	3000	

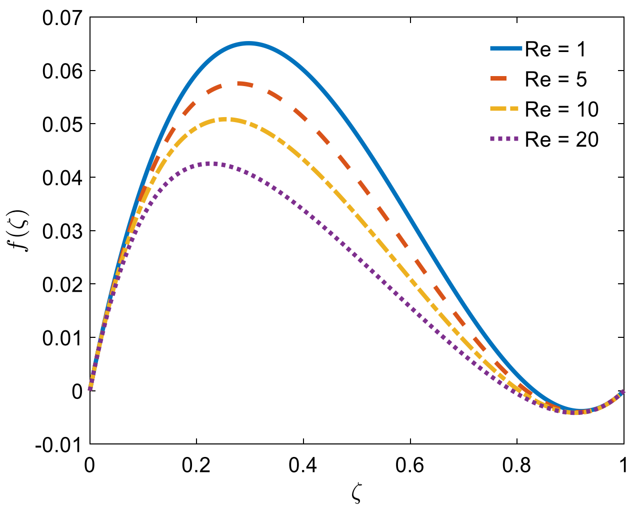

Fig. 3 Impact of *Re* on *f*.

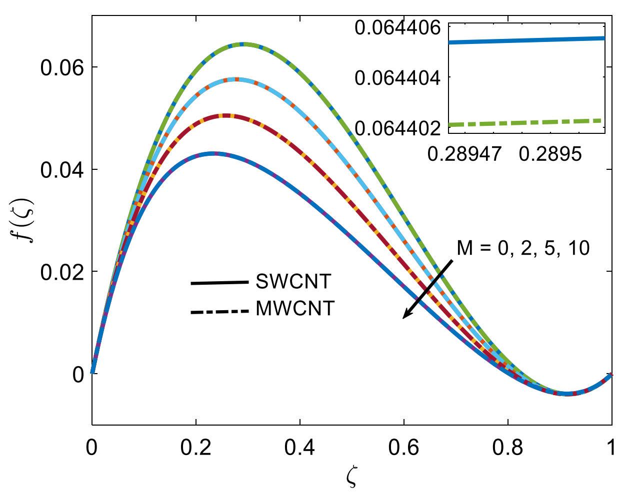

Fig. 4 Impact of *M* and nature of nanoparticles on *f*.

the flow of CNT-water nfs structured with interfacial nanolayer. Fig. 3 illustrates that increase in *Re* peters out the axial velocity $f(\zeta)$ at lower disk (LD) while at upper disk (UD) the magnitude of $f(\zeta)$ gets reduced. In the absence of external magnetic field i.e., in the hydrodynamic flow ($M = 0$), $f(\zeta)$ was with greater value. In the presence of magnetic field strength i.e., in the MHD flow ($M \neq 0$), $f(\zeta)$ follows a decelerated flow pattern both at lower and upper disks. However, $f(\zeta)$ possesses lower magnitude at the UD than that at LD (Fig. 4). How did

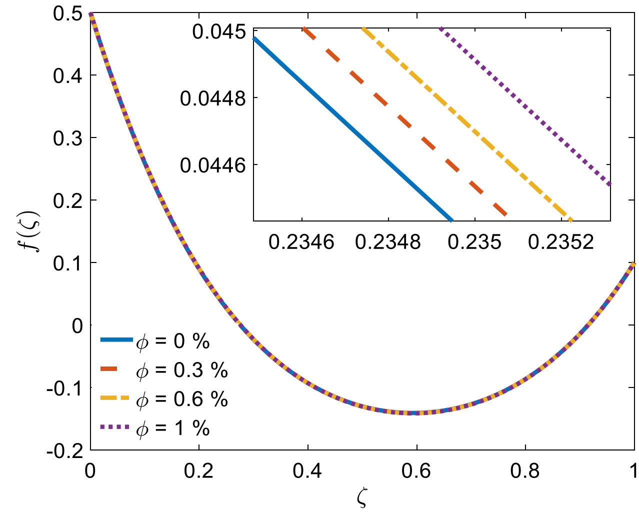

Fig. 5 Impact of ϕ on *f*.

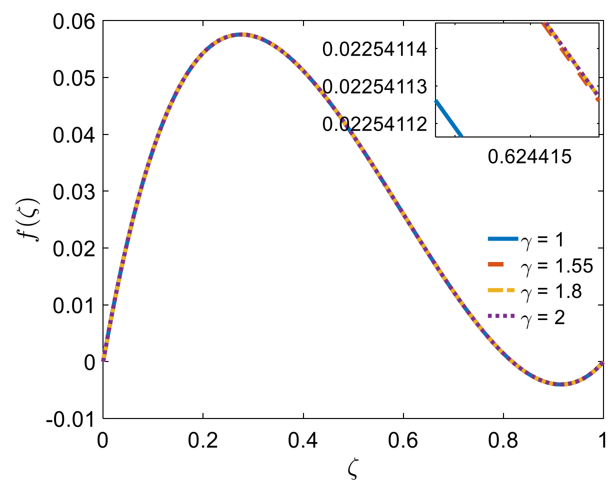

Fig. 6 Impact of shape factor γ on *f*.

the decay occur? The inhibition of Lorentz force is realized. Lorentz force resists the motion of the conducting CNT-water nf, therefore, decelerated flow situation is the expected outcome. Impact of nanoparticle volume fraction $\phi(\phi = 0, 0.3, 0.6, 1)$ on $f(\zeta)$ is demonstrated in Fig. 5. In case of base fluid ($\phi = 0\%$), the magnitude of $f(\zeta)$ was low. With the insertion of CNTs as nanoparticles, $f(\zeta)$ gets augmented, though marginally at both disks. In fact, UD moves with axial velocity greater than that of LD (Fig. 5). The influence of shape factor $\gamma(\gamma = 1,\ 1.55,\ 1.8,\ 2)$ on $f(\zeta)$ is well depicted in Fig. 6. It is understood that rise in γ with varied shape of nanoparticles an accelerated flow along axial direction is achieved for both LD and UD.

5.2. Radial velocity characteristics

This section enshrines the valuable contributions of the important embedded parameters to the radial velocity field. Fig. 7 witnesses that the radial velocity $f'(\zeta)$ of CNT-water nf gets declined at LD due to rise of *Re*. There is a reflection point

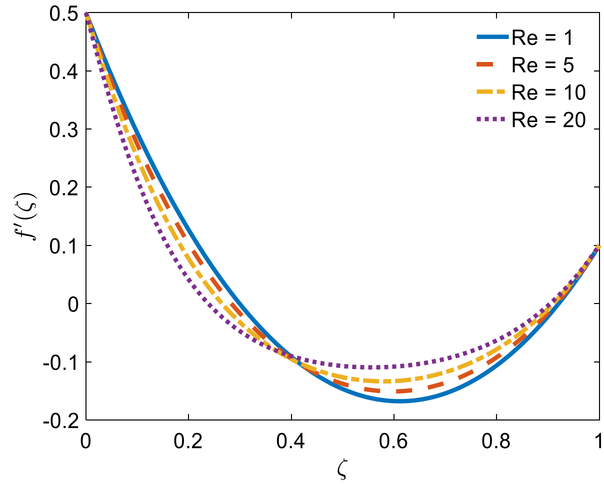

Fig. 7 Impact of Re on f'.

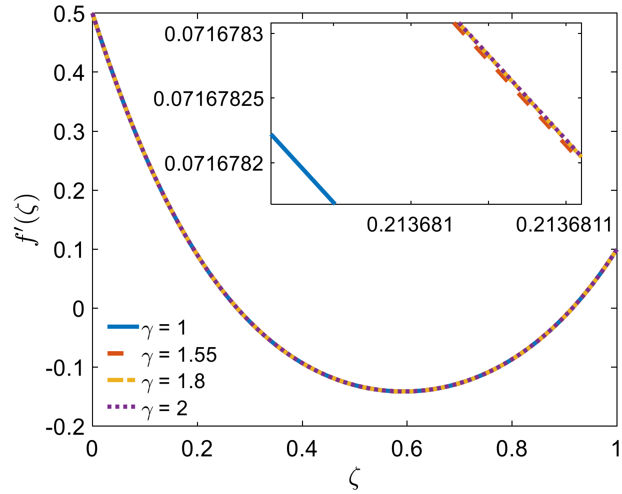

Fig. 9 Impact of shape factor γ on f'.

near $\eta = 0.4$. An opposite trend is attained beyond that point (for UD). As Re is raised the inertial effect due to rotation of LD enhances which in turn causes the flow to sluggish. Negative values of $f'(\zeta)$ demonstrates that the UD moves faster than LD. The physical rationale behind it is that the raising the values of magnetic field retards the motion of CNT-water nf. This is evident from Javed et al. [29]]. Further the decelerated flow is greater for SWCNT than that of MWCNT while the accelerated flow is greater for MWCNT than that of SWCNT. In the absence of stretching ($A_1 = 0$) of LD, $f'(\zeta)$ vanishes for LD and is insignificant for UD (due to rotation). As A_1 is raised, $f'(\zeta)$ seemingly strengthens near LD while it exhibits a downward trend near UD (Fig. 8). Negative values of $f'(\zeta)$ at LD is meant to ensure that UD moves faster than the LD. Increase in $\gamma(\gamma = 1,\ 1.55,\ 1.8,\ 2)$ yields marginally accelerated flow near the LD and UD (Fig. 9).

5.3. Tangential velocity characteristics

In this section, the real nature of tangential velocity under the impact of influencing parameters has been described in very lucid manner. In the absence of thermal buoyancy ($Gr = 0$), $g(\zeta)$ was low. Increase of $Gr(Gr = 0, 0.5, 1, 2)$ has played a role in the increase of $g(\zeta)$ for both LD and UD (Fig. 10). In hydrodynamic flow ($M = 0$), $g(\zeta)$ attains high value at LD and low value at UD. However, for MHD flow ($M \neq 0$), $g(\zeta)$ declines near LD indicating decelerated flow there and yields a persistent upward trend near UD (beyond the reflection point near $\eta = 0.3$)indicating accelerated flow there. No significant variations appear in both types of flows for SWCNT and MWCNT (Fig. 11). In the absence of inertia ($F_r = 0$), $g(\zeta)$ is low for both disks. With the raise of $F_r(F_r = 0,\ 0.5,\ 1, 2)$, $g(\zeta)$ peters out (Fig. 12). With no stretching of LD ($A_1 = 0$), $g(\zeta)$ has greater magnitude for both disks. However, due to gradual increase of stretching of LD ($A_1 = 0, 0.2, 0.5, 0.8$), $g(\zeta)$ gets diminution for both disks. It is envisioned that $g(\zeta)$ profiles merge at $\zeta = 1$. This implicates that $g(\zeta)$ attains a saturated value $g(\zeta) = 0.5$ unit above the surface of UD (Fig. 13).

5.4. Thermal characteristics

This section focuses on the exploration regarding the thermal characteristics due to the flow of CNT-water nfs in the pres-

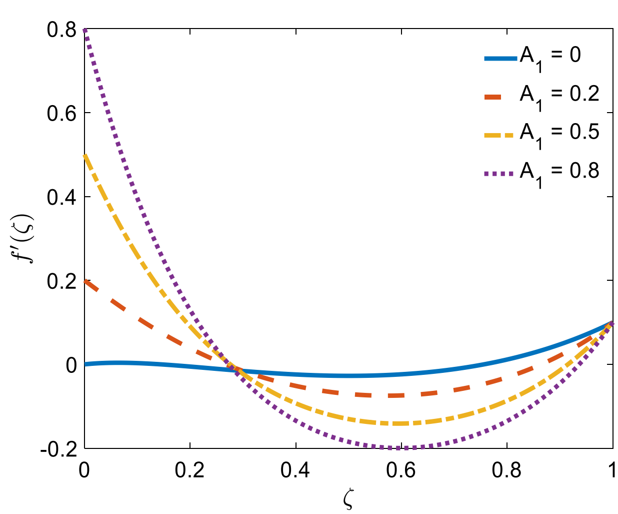

Fig. 8 Impact of A_1 on f'.

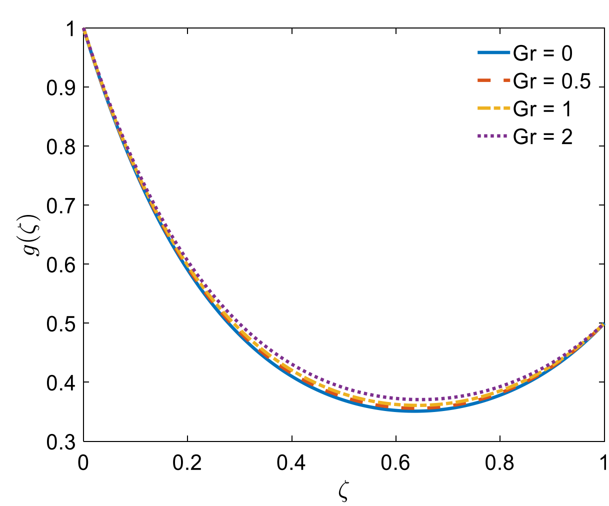

Fig. 10 Impact of Gr on $g(\zeta)$.

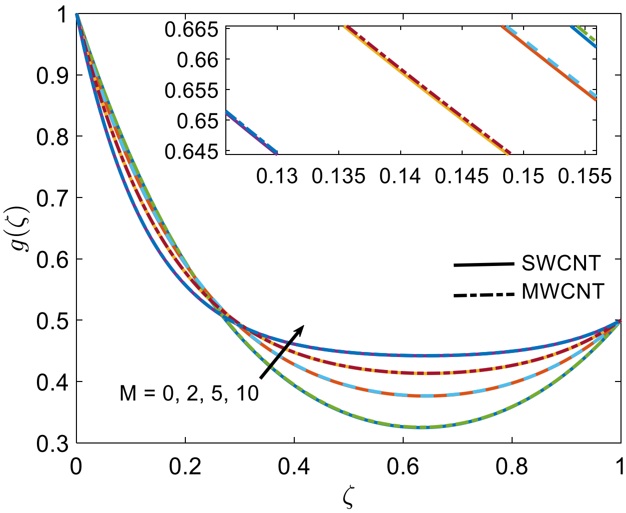

Fig. 11 Impact of M on $g(\zeta)$ for SWCNT and MWCNT nps.

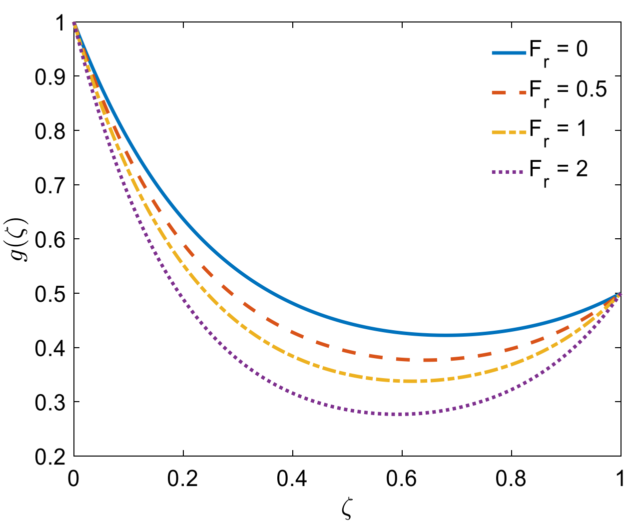

Fig. 12 Impact of F_r on $g(\zeta)$.

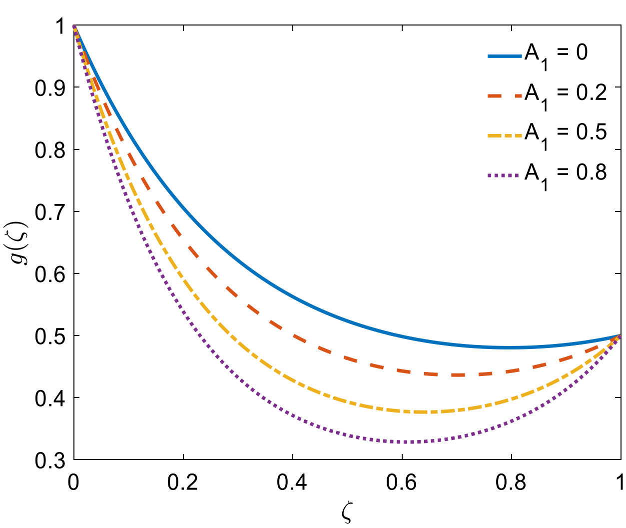

Fig. 13 Impact of A_1 on $g(\zeta)$.

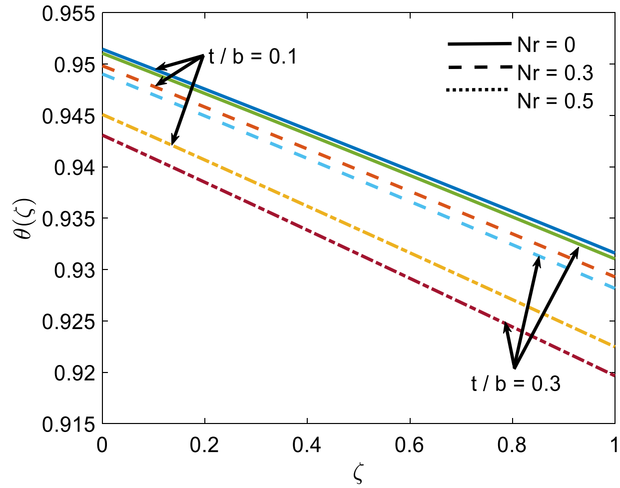

Fig. 14 Impact of Nr and t/b on $\theta(\zeta)$.

ence of interfacial nanolayer subject to varied shape of nanoparticles. The behavior of fluid temperature $\theta(\zeta)$ for varied estimations of interfacial ratio parameter $\left(\frac{t}{b}\right)\left(\frac{t}{b}=0.1,0.3\right)$ and $Nr(Nr=0,0.3,0.5)$ is understood from the sight (Fig. 14) clearly. A rise in $\left(\frac{t}{b}\right)$ declines $\theta(\zeta)$ and hence augments the rate of heat transportation (HT) into the nf. Further, rise in TR (increase in Nr) decays $\theta(\zeta)$ and the related BLT. The influence of $\left(\frac{t}{b}\right)$ and ϕ on $\theta(\zeta)$ is illustrated in Fig. 15. Augmented $\left(\frac{t}{b}\right)$ reduces $\theta(\zeta)$. Further, at each $\left(\frac{t}{b}\right)$(for instance at $\frac{t}{b}=0.1$), rise in $\phi(\phi=0.01,0.03,0.05,0.08)$ upsurges $\theta(\zeta)$ and the related BLT i.e.,

$\theta(\zeta)|_{\phi=0.01}<\theta(\zeta)|_{\phi=0.03}<\theta(\zeta)|_{\phi=0.05}<\theta(\zeta)|_{\phi=0.08}$ at $\frac{t}{b}=0.1$. Influence of ϕ on $\theta(\zeta)$ for both SWCNT and MWCNT is visualized in Fig. 16. As ϕ rises, $\theta(\zeta)$ augments for SWCNT-water and MWCNT-water nfs near both LD and UD. Physically, rise in the volume fraction of nps implicating their more thermal conductivity which in turn causes more heat to penetrate more into the quiescent. This is evident from Mustafa et al. [35]. There are indications that the magnitude of $\theta(\zeta)$ is low for SWCNT-water nf than that of MWCNT-water nf. Increase in M peters out $\theta(\zeta)$ for both SWCNT and MWCNT nfs at LD and UD. However, the decay is more for SWCNT–

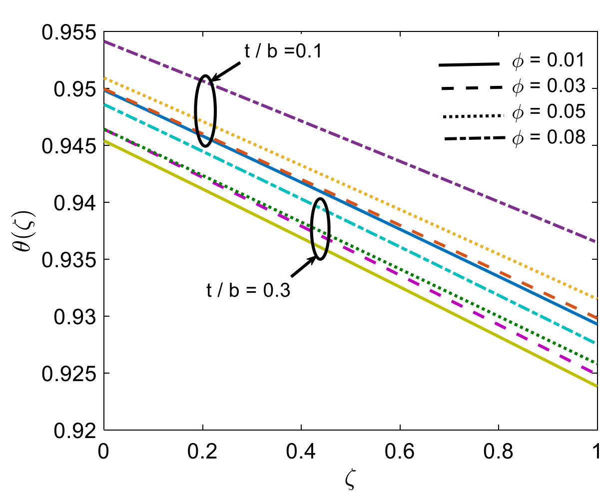

Fig. 15 Impact of ϕ and t/b on $\theta(\zeta)$(about t/b).

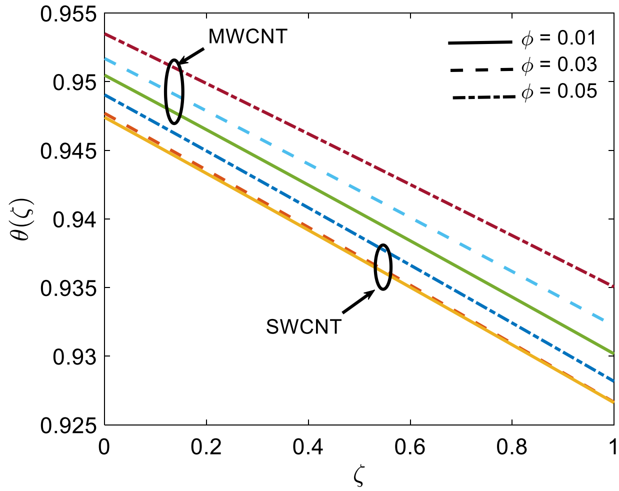

Fig. 16 Impact of ϕ on $\theta(\zeta)$ for SWCNT and MWCNT.

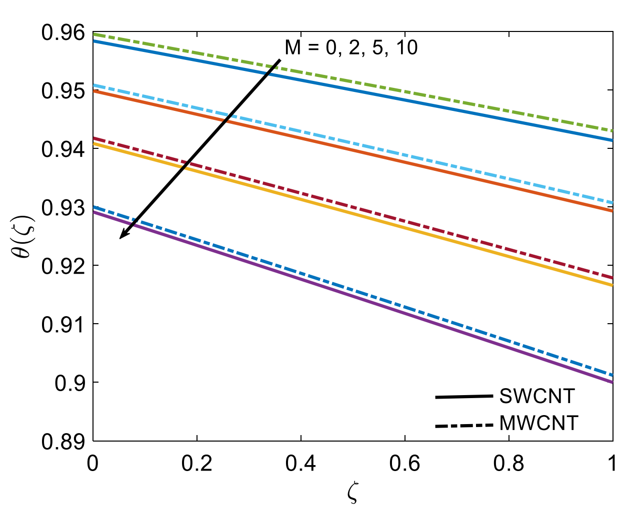

Fig. 17 Impact of M on $\theta(\zeta)$ for SWCNT and MWCNT.

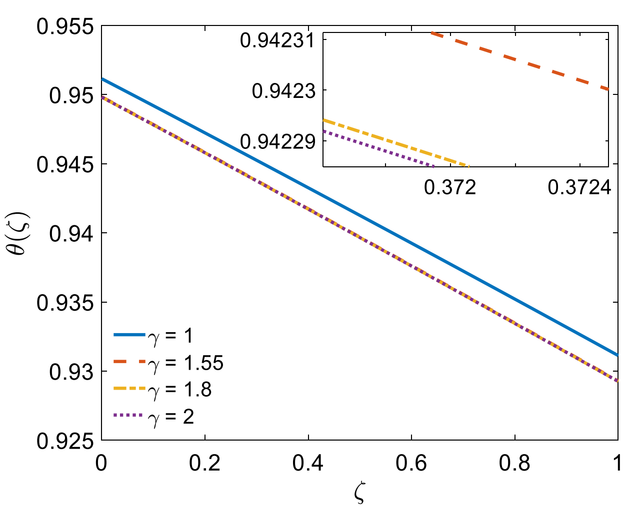

Fig. 18 Impact of shape factor γ on $\theta(\zeta)$.

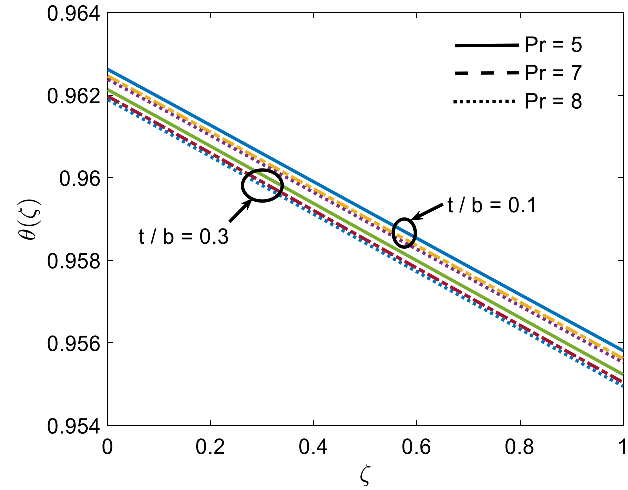

Fig. 19 Impact of Pr and t/b on $\theta(\zeta)$.

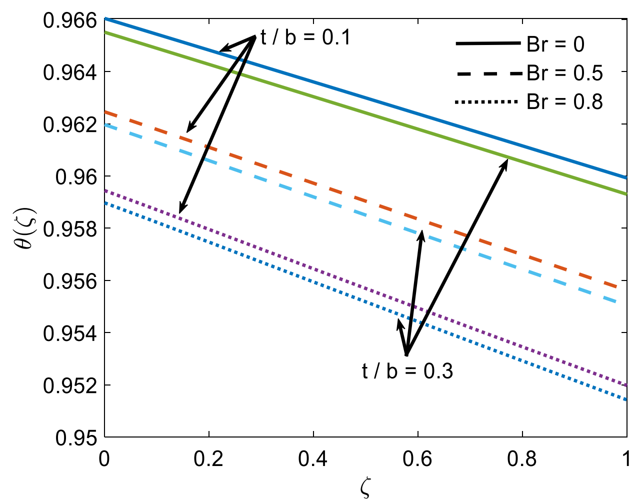

Fig. 20 Impact of Br and t/b on $\theta(\zeta)$.

water than that of MWCNT-water nfs (Fig. 17). Augmented γ peters out $\theta(\zeta)$ near both the disks (Fig. 18). Higher Prandtl fluid (more Pr) contributes to low $\theta(\zeta)$ and the shrinkage of TBL. Low Prandtl fluid promotes to high $\theta(\zeta)$. Regardless the nature of Prandtl fluid (low or high), rise in $\left(\frac{t}{b}\right)$ has resulted in decline of $\theta(\zeta)$ for both LD and UD (Fig. 19). At each Prandtl fluid $\theta(\zeta)$ is high for LD and low for UD.Fig. 26 addresses that $\theta(\zeta)$ belittles due to rise in $\left(\frac{t}{b}\right)$. At each $\left(\frac{t}{b}\right)$, null Br yields maximum $\theta(\zeta)$ and rise of Br causes $\theta(\zeta)$ to decay. This results in significant rate of HT from the LD as well as UD. However, the values of $\theta(\zeta)$ are less near UD (Fig. 20). This is because Brinkman number (Br) and thermal conductivity $\left(k_{nf}\right)$ have inverse relation. Therefore, for rising values of (Br), the thermal conductivity $\left(k_{nf}\right)$ d1rop down which in turn-belittles the temperature. This is well agreed with Hayat et al. [37]. Regardless $\left(\frac{t}{b}\right)$ value, increase in θ_r diminishes $\theta(\zeta)$ and the related BLT and consequently enhances the HTR (Fig. 21). Incremented convective heating (rise in B_1) reduces $\theta(\zeta)$ and the related BLT (Fig. 22). Further, Fig. 23 reveals that increase in $\left(\frac{t}{b}\right)$ yields fall in $\theta(\zeta)$. At each $\left(\frac{t}{b}\right)$, increase in B_2 belittles $\theta(\zeta)$ with lower magnitude near the UD.

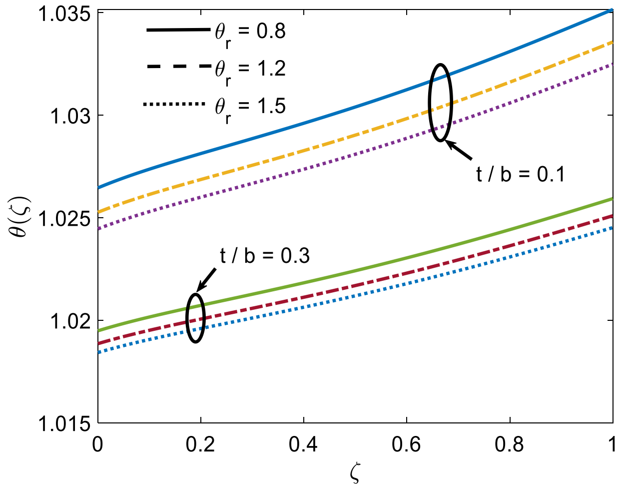

Fig. 21 Impact of θ_r and t/b on $\theta(\zeta)$.

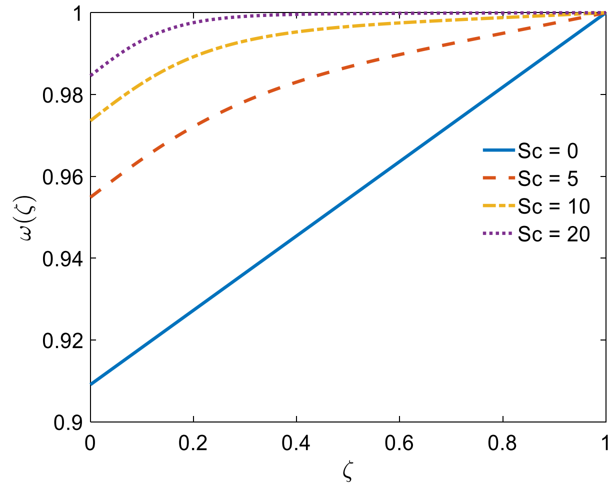

Fig. 24 Impact of Sc on $\omega(\zeta)$.

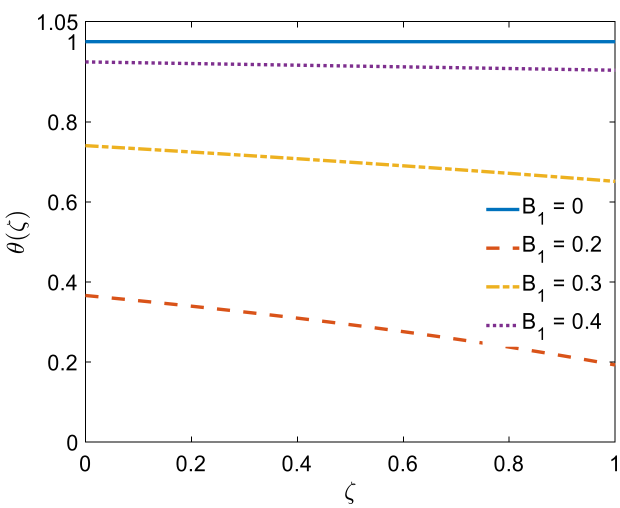

Fig. 22 Impact of B_1 on $\theta(\zeta)$.

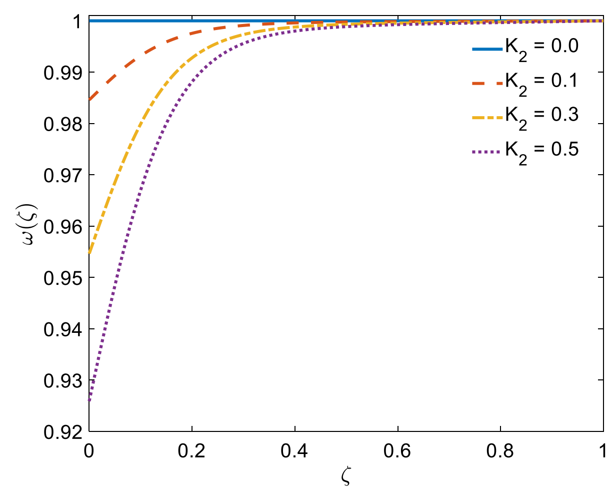

Fig. 25 Impact of K_2 on $\omega(\zeta)$.

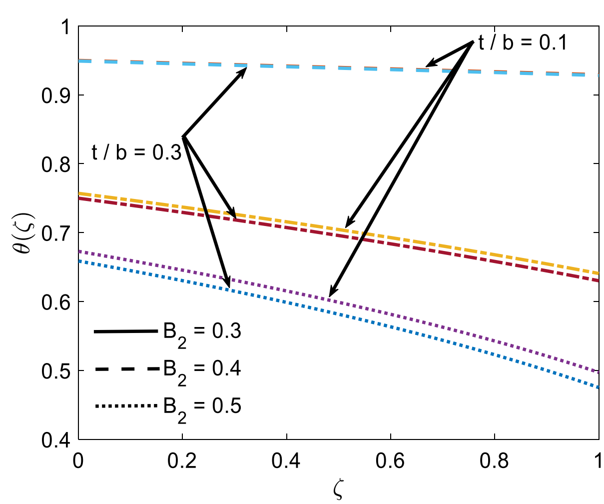

Fig. 23 Impact of B_2 and t/b on $\theta(\zeta)$.

5.5. Nanoparticles concentration characteristics

This section reflects the nps concentration behavior in relation to associated parameters. Fig. 24 demonstrates the nature of nps concentration $\omega(\zeta)$ in relation to the absence and presence of $Sc(Sc = 0$ and $Sc \neq 0)$. As Sc is raised, $\omega(\zeta)$ sharply enhances providing significant accumulation of nps concentration. In the absence of heterogeneous reaction $(K_2 = 0)$, $\omega(\zeta)$ was very high, however, with increase of K_2(in the presence of more and more heterogeneous reaction), there has been substantial increasing of $\omega(\zeta)$ and the related BLT (Fig. 25). Rise in γ uplifts $\omega(\zeta)$(Fig. 26).

5.6. Surface viscous drag and HTR characteristics

In this section, surface viscous drag and HTR characteristics due to the influence pertinent parameters have been narrated. As Gr is augmented, skin friction coefficient $\{C_f(0)\}$ decays. This implicates that the viscous drag diminishes at the surface of both LD and UD with increase of thermal buoyancy in the presence of interfacial nanolayer (Figs. 27 and 28). Table 2

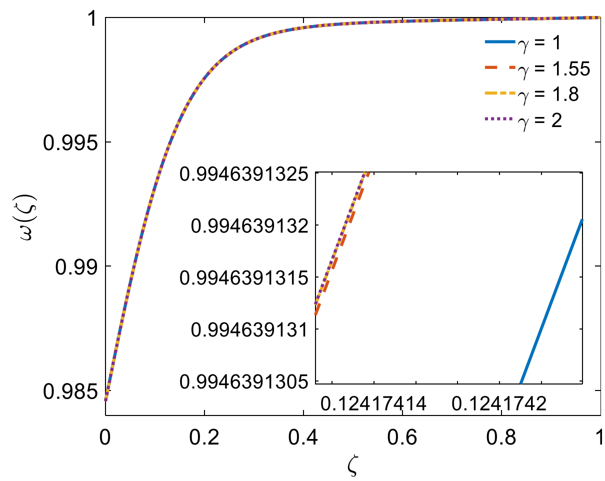

Fig. 26 Impact of γ on $\omega(\zeta)$.

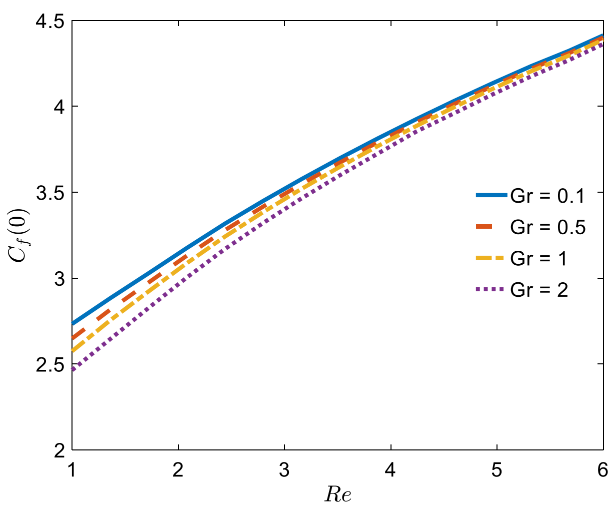

Fig. 27 Impact of Gr on $C_f(0)$ against Re.

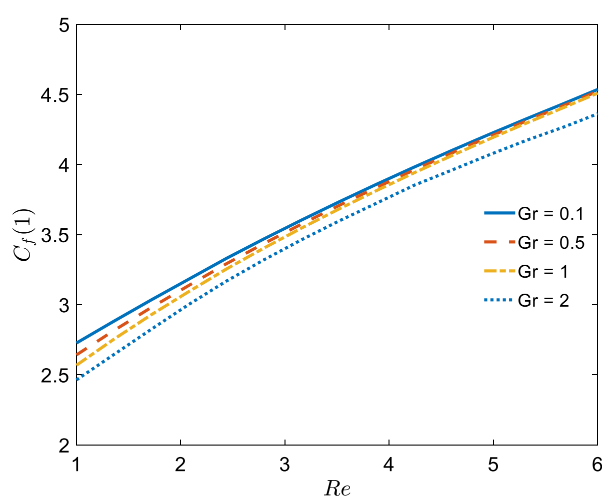

Fig. 28 Impact of Gr on $C_f(1)$ against Re.

reveals that increase in $Re(Re = 5, 10, 20)$ has amplified on the effects of surface viscous drag (SVD) $\{C_f(0)\}$ for LD and $\{C_f(1)\}$ for UD. When thermal buoyancy rises (Gr increases), $\{C_f(0)\}$ and $\{C_f(1)\}$ diminish as expected (Table 2). In the light of increment of F_r, A_1, A_2, SVD $\{C_f(0)\}$ and $\{C_f(1)\}$ upgrade their values while they peter out due to rise in M(Table 2). The rate of HT peters out from the surface of LD within the strength $M = 2$ unit. Beyond this strength, the rate of HT exhibits upward trend (Fig. 29). The rate of HT follows the same trend from the surface of UD with the presence of interfacial nanolayer (Fig. 30). Influence of Br on HTR against ϕ from LD and UD is visualized in Figs. 31 and 32. From Fig. 31 it is obvious that in the marginal viscous heating with specific conduction through particles, HTR from the LD $\{Nu_r(0)\}$ upsurges for $0 \leqslant \phi \leqslant 0.06$. However, for nps beyond $\phi = 0.06$, reverse nature is the result (Fig. 32). In addition, Table 3 conveys that rise in Nr, Pr, Re, Br and E_1 uplifts the HTR and that of θ_r and M belittles HTR from the surface of LD and UD $\{Nu_r(1)\}$.

5.7. Entropy generation number and Bejan number characteristics

In this section the role of different parameters on EGN and Bejan number characteristics in the flow of CNT-water nfs in the presence of interfacial nanolayer has been explored. The EG due to LD augments rhythmically with increase in $\beta_1(\beta_1 = 0.1, 0.3, 0.5, 0.8)$ for different values of inertia coefficient (F_r) as is envisioned in Fig. 33. Exactly, opposite characteristic (descending trend) of $\{N_G(0)\}$ is obtained due to rise in $\alpha(\alpha = 0.1, 0.2, 0.5, 0.8)$ for different Re (Fig. 34). The variation of Bejan number from the surface of LD, $\{Be(0)\}$ for different estimations of $\beta_1(\beta_1 = 0.1, 0.3, 0.5, 0.8)$ against F_r is shown in Fig. 35. Here, $\{Be(0)\}$ gets augmented due to rising β_1 for different F_r. The Bejan number due to LD i.e., $\{Be(0)\}$ declines with rise in $\alpha(\alpha = 0.1, 0.2, 0.5, 0.8)$ for different Re(Fig. 36). Table 4 ensures us that raise in α causes the EGN $\{N_G(0)\}$ and Bejan number $\{Be(0)\}$ to belittle near LD and uplift EGN $\{N_G(1)\}$ and Bejan number $\{Be(1)\}$ near the UD. Exactly the opposite behavior is the outcome due to the impact of rise in Re. Rise in Nr and Br upgrades $\{N_G(0)\}$ due to LD. However, rise in Nr and Br develop opposite trend for $\{Be(0)\}$ on the surface of LD. Further, hike in Nr and Br enhances $\{N_G(1)\}$ on the surface of the UD while that of Nr and Br show the behavior opposite to each other on the surface of UD. In addition, rise in β_1 and β_2 contributes to growth of $\{N_G(0)\}$ and $\{Be(0)\}$ on LD and $\{N_G(1)\}$ and $\{Be(1)\}$ on UD. Hike in ϕ gets diminution in $\{N_G(0)\}$ and $\{N_G(1)\}$ on the surface of LD and UD respectively. An exactly opposite trend is visualized for $\{Be(0)\}$ and $\{Be(1)\}$ on the surface of LD and UD respectively.

6. Conclusions

In the present investigation the influence of interfacial nanolayer and shape effects using revised Hamilton-Crosser model in the Darcy Forchheimer electromagnetic flow of SWCNT/MWCNT-water nanofluid subject to nonlinear thermal radiation and chemical reactions has been analyzed. The principal outcomes of the above said analysis include:

Table 2 Skin friction at the surface of LD$\left(C_f(0)\right)$ and UD$\left(C_f(1)\right)$ for different parameters with $\theta_r = 10$.

Re	*Gr*	F_r	*M*	A_1	A_2	$C_f(0)$	$C_f(1)$
5	0.5	0.5	2	0.5	0.1	4.21964858	1.16812069
10						5.58825749	1.73591761
20						7.60156551	1.98865035
	1					4.20311019	1.17474463
	2					4.17021621	1.14961914
		1				4.51597000	1.23689116
		2				5.06899600	1.29534953
			5			5.05615110	0.90651101
			8			5.78856995	0.71803952
				0.2		2.71434494	0.86792584
				0.8		6.14616331	1.90121629
					0.5	4.68222248	1.89513579
					0.8	5.02535086	1.99399042

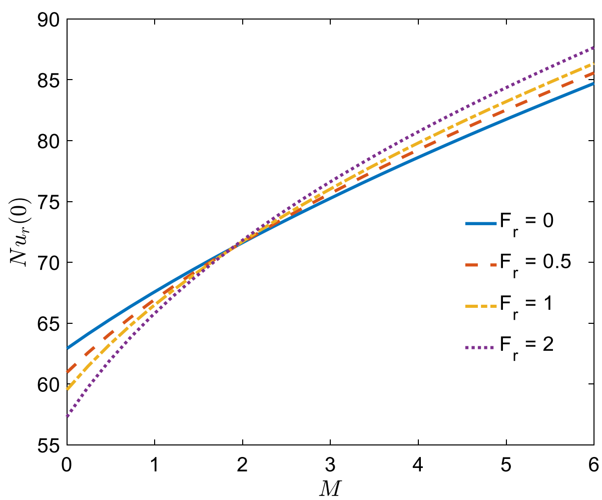

Fig. 29 Impact of F_r on $Nu_r(0)$ against M.

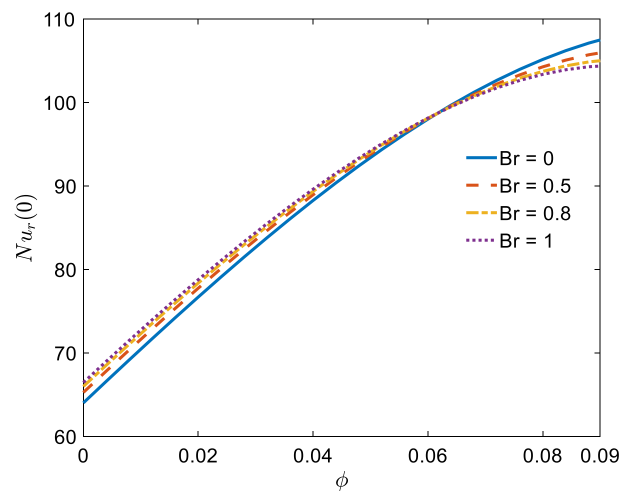

Fig. 31 Impact of Br on $Nu_r(0)$ against ϕ.

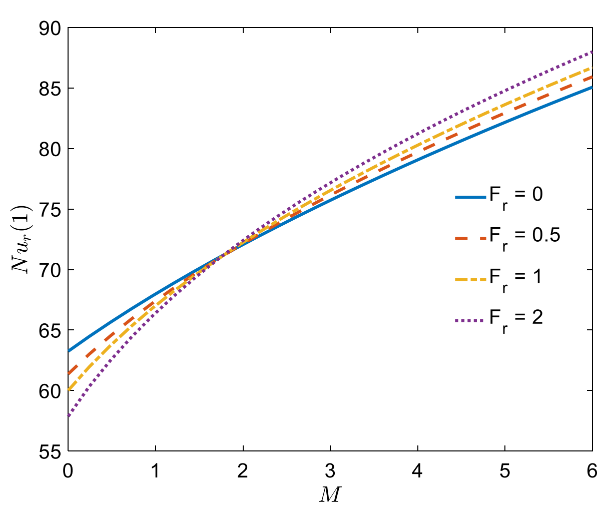

Fig. 30 Impact of F_r on $Nu_r(1)$ against M.

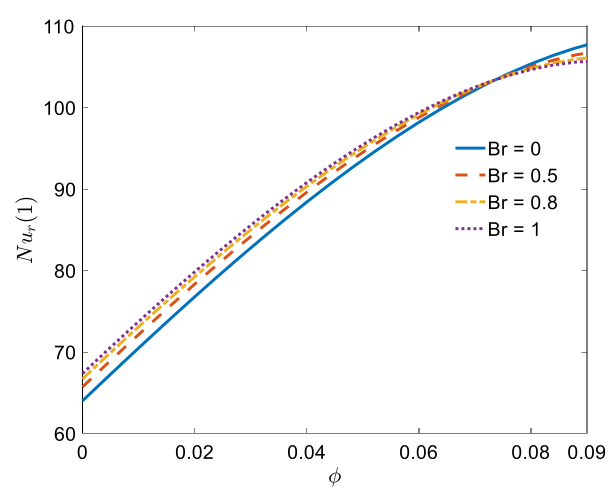

Fig. 32 Impact of Br on $Nu_r(1)$ against ϕ.

Table 3 Local Nusselt number at the surface of LD($Nu_r(0)$) and UD($Nu_r(1)$) cylinders for different parameters with $\theta_r = 1.2$.

Nr	Pr	Re	Br	M	E_1	$Nu_r(0)$	$Nu_r(1)$
0.2	7	5	0.5	2	0.5	2.74026638	1.92929589
0.5						2.76561794	1.94676197
0.8						2.77215871	1.95127512
	6					2.76753433	1.95730672
	8					2.71372152	1.90202813
		6				7.45133693	6.61919303
		7				12.09570393	11.22017364
			0.8			4.37173116	3.06600429
			1			5.45412909	3.79312514
				4		10.78439245	9.92174800
				6		18.68895625	17.77800766
					0.6	16.75077961	16.16946541
					0.7	32.97418283	32.67730168

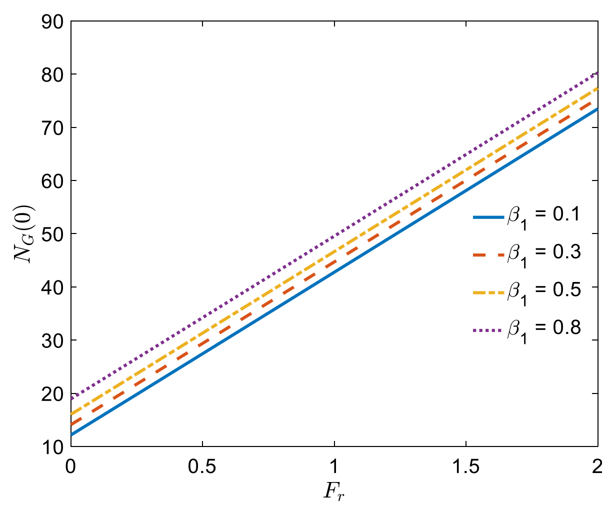

Fig. 33 Impact of β_1 on $N_G(0)$ against F_r.

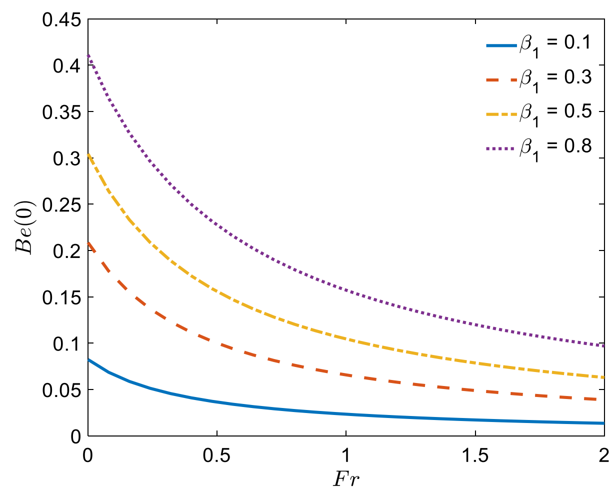

Fig. 35 Impact of β_1 on $Be(0)$ against F_r.

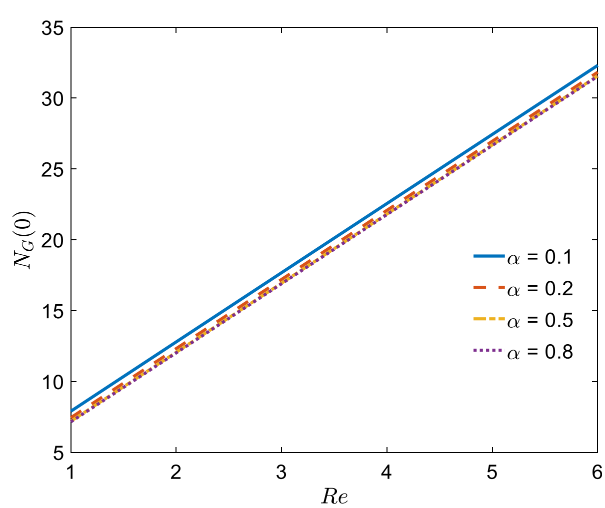

Fig. 34 Impact of α on $N_G(0)$ against Re.

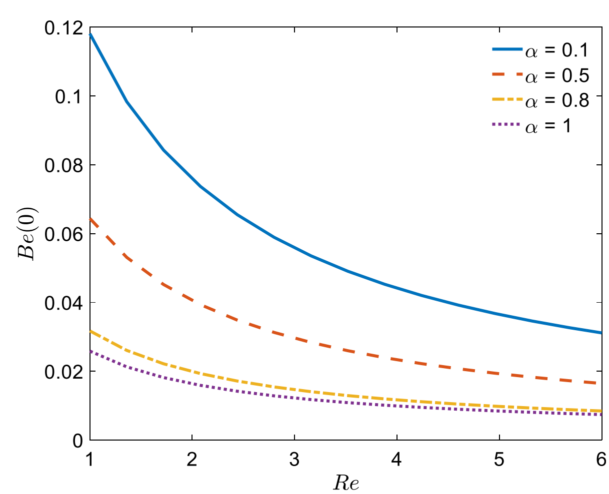

Fig. 36 Impact of α on $Be(0)$ against Re.

Table 4 Entropy generation and Bejan numbers at the surface of LD$(N_G(0), Be(0))$ and UD $(N_G(1), Be(1))$ for different parameters with $\theta_r = 10$.

α	Nr	Br	Re	β_1	β_2	ϕ	$N_G(0)$	$Be(0)$	$N_G(1)$	$Be(1)$
0.1	0.2	0.5	5	0.1	0.2	0.1	27.44017816	0.03650967	1.37576371	0.00486343
0.2							26.95834500	0.01928897	1.37419413	0.00372680
0.3							26.80617127	0.01372165	1.37446122	0.00392040
	0.5						27.44318050	0.03660152	1.37583135	0.00488973
	0.8						27.44650823	0.03670498	1.37584885	0.00489657
		0.8					43.30352567	0.02314155	2.44085685	0.00395896
		1					53.87911296	0.01860265	4.94021898	0.09079298
			10				51.10809119	0.00720344	6.28114612	0.87922497
			20				99.94461575	0.00743895	3.18114610	0.41979412
				0.5			31.31696610	0.15578201	1.40464281	0.02871033
				0.8			34.22455705	0.22750362	1.42079726	0.03975388
					0.5		27.47014656	0.03756079	1.38331247	0.01373328
					0.8		27.50011495	0.03860961	1.38352140	0.01388222
						0.2	20.40892816	0.04908792	0.68317391	0.02750176
						0.3	18.06517816	0.05545652	0.44986403	0.04176481

- Greater strength of external magnetic field controls the axial, radial and tangential motion of CNT-water nanofluid.
- With gradual increase of stretching of LD (rise in A_1), $f(\zeta)$ and $f'(\zeta)$ augment at LD and peters out at UD. However, its influence belittles $g(\zeta)$ for both LD and UD. Further, gradual stretching of UD (rise in A_2), yields diminution of $f(\zeta)$ and $f'(\zeta)$ at LD while showing up gradation in UD.
- Enhanced shape factor of nanoparticles (hike in γ) leads to accelerated flow along axial and radial directions while yields decelerated flow along tangential direction.
- Incremented interfacial layer parameter (increase in $\frac{t}{b}$) augments HTR from the surfaces of LD and UD.
- Rise in ϕ gives rise to intensify $\theta(\eta)$ and the related TBL.
- Hiked K_2 raised $\omega(\zeta)$ and the related BLT.
- Incremented Fr, A_1, A_2 resulted in upgraded $\{C_f(0)\}$ and $\{C_f(1)\}$ for CNT-water nf.
- Mounted $Nr, \Pr, Re, Br$ and E_1 upgraded HTR while that of θ_r and M slows down HTRfrom the surfaces of LD and UD.
- Rise in Nr and Br uplifts $\{N_G(0)\}$ and declines $\{N_G(1)\}$.

Declaration of Competing Interest

The authors declared that they have no conflict of interest and the paper presents their own work which does not been infringe any third-party rights, especially authorship of any part of the article is an original contribution, not published before and not being under consideration for publication elsewhere.

References

[1] Muhammad Imran Asjad, Muhammadish Danish Ikram, Ali Akgül, Analysis of MHD viscous fluid flow through porous medium with novel power law fractional differential operator, Phys. Scr. 95 (2020) 115209.

[2] Ali Akgül, Imran Siddique, Novel applications of the magnetohydrodynamics couple stress fluid flows between two plates with fractal-fractional derivatives, Numer. Methods Partial Differential Equations (2020), https://doi.org/10.1002/num.22673.

[3] Rizwan Ali, Ali Akgül and Muhammad Imran Asjad, Power law memory of natural convection flow of hybrid nanofluids with constant proportional Caputo fractional derivative due to pressure gradient, Pramana – J. Phys. 94 (2020) 131.

[4] Gulzar Ahmad Danish, M. Imran, Madeeha Tahir, M.I. Asjad HassanWaqas, Ali Akgül, Dumitru Baleanu, Effects of Non-Linear Thermal Radiation and Chemical Reaction on Time Dependent Flow of Williamson Nanofluid With Combine Electrical MHD and Activation Energy, J. Appl Comput. Mech. (2021) 1–13, https://doi.org/10.22055/JACM.2020.35122.2568.

[5] M.K. Nayak, T.M. Agbaje, S. Mondal, P. Sibanda, P.G.L. Leach, Thermodynamic effect in Darchy-Forchheimer nanofluid flow of a single-wall carbon nanotube/multi-wall carbon nanotube suspension due to a stretching/shrinking rotating disk: Buongiorno two-phase model, J. Eng. Math. (2020), https://doi.org/10.1007/s10665-019-10031-9.

[6] T. Hayat, M. Javed, M. Imtiaz, A. Alsaedi, Convective flow of Jeffrey nanofluid due to two stretchable rotating disks, J. Mol. Liq., doi: 10.1016/j.molliq.2017.05.024.

[7] S. Mosayebidorcheh, M. Hatami, Heat transfer analysis in carbon nanotube-water between rotating disks under thermal radiation conditions, J of Mol. Liq., doi: 10.1016/j.molliq.2017.05.085.

[8] H. Jiang, Q. Xu, C. Huang, L. Shi, The role of interfacial nanolayer in the enhanced thermal conductivity of carbon nanotube-based nanofluids, Appl. Phys. A 118 (1) (2015) 197–205.

[9] S. Murshed, C. Nieto de Castro, Superior thermal features of carbon nanotubes based nanofluids – a review, Renew. Sustain. Energy Rev. 37 (2014) 155–167.

[10] R. Sadri, G. Ahmadi, H. Togun, M. Dahari, S.N. Kazi, E. Sadeghinezhad, N. Zubir, An experimental study on thermal conductivity and viscosity of nanofluids containing carbon nanotubes, Nanoscale Res. Lett. 9 (1) (2014) 151.

[11] S. Choi, Z. Zhang, W. Yu, F. Lockwood, E. Grulke, Anomalous thermal conductivity enhancement in nanotube suspensions, Appl. Phys. Lett. 79 (14) (2001) 2252–2254.

[12] S. Nadeem, Iqra shahzadi, Single wall carbon nanotube (SWCNT) analysis on peristaltic flow in an inclined tube with permeable walls, Int. J. Heat Mass Transf. 97 (June 2016) 794–802.

[13] B. Mahanthesh, B.J. Gireesha, N.S. Shashikumar, S.A. Shehzad, Marangoni convective MHD flow of SWCNT and MWCNT nanoliquids due to a disk with solar radiation and irregular heat source, Physica E 94 (October 2017) 25–30.
[14] Sohail Ahmed, Hang Xu, Qiang Sun, Stagnation Flow of a SWCNT Nanofluid towards a Plane Surface with Heterogeneous-Homogeneous Reactions, Math. Problems Eng., Volume 2020 |Article ID 3265143.
[15] Santosh Chaudhary, K.M. Kanika, Radiation heat transfer on SWCNT and MWCNT based magnetohydrodynamic nanofluid flow with marangoni convection, Phys. Scr. 95 (2020) 025202.
[16] A. Shahsavar, M. Bahiraei, Experimental investigation and modeling of thermal conductivity and viscosity for non-Newtonian hybrid nanofluid containing coated CNT/Fe3O4 nanoparticles, Powder Technol. 318 (2017) 441–450.
[17] Sabir Ali Shehzad, Basavarajappa Mahanthesh, Bijjanal Jayanna Gireesha, Nagavangala Shankarappa Shashikumar, Macha Madhu, Brinkman-Forchheimer slip flow subject to exponential space and thermal-dependent heat source in a microchannel utilizing SWCNT and MWCNT nanoliquids, Heat Transfer Asian Res. 48(5) (2019) 1688-1708.
[18] Abdullah Dawar, Zahir Shah, Waris Khan, Muhammad Idrees, Saeed Islam, Unsteady squeezing flow of magnetohydrodynamic carbon nanotube nanofluid in rotating channels with entropy generation andviscous dissipation, Adv. Mech. Eng. 11 (1) (2019) 1–18.
[19] A. Bejan, Entropy generation through heat and fluid flow Wiley, New York (1982).
[20] S. Farooq, M. Ijaz Khan, M. Waqas, T. Hayat, A. Alsaedi, Transport of hybrid type nanomaterials in peristaltic activity of viscous fluid considering nonlinear radiation, entropy optimization and slip effects, Comput. Meth. Progr. Bio. 184 (2020) 105086.
[21] M.K. Nayak, A.K. Abdul Hakeem, B. Ganga, M. Ijaz Khan, M. Waqas, O.D. Makinde, Entropy optimized MHD 3D nanomaterial of non-Newtonian fluid: A combined approach to good absorber of solar energy and intensification of heat transport, Comput. Meth. Progr. Bio. 186 (2020) 105131.
[22] M. Waleed Ahmad Khan, M. Ijaz Khan, T. Hayat, A. Alsaedi, Numerical solution of MHD flow of power law fluid subject to convective boundary conditions and entropy generation, Comp. Meth. Prog.Biomed. 186 (2020) 105131. Doi: https://doi.org/10.1016/j.cmpb.2019.105262.
[23] A.J. Chamkha, A.M. Rashad, M.A. Mansour, T. Armaghani, M. Ghalambaz, Effects of heat sink and source and entropy generation on MHD mixed convection of a Cu-water nanofluid in a lid-driven square porous enclosure with partial slip, Phys. Fluids 29 (2017) 052001.
[24] M.I. Afridi, I. Tlili, M. Qasim, I. Khan, Nonlinear Rosseland thermal radiation and energy dissipation effects on entropy generation in CNTs suspended nanofluids flow over a thin needle, Boundary Value Problems 2018 (2018) 148.
[25] M. Waleed Ahmed Khan, M. IjazKhana, T. Hayat, A. Alsaedi, Entropy generation minimization (EGM) of nanofluid flow by a thin moving needle with nonlinear thermal radiation, Phys. B: Condens. Matter 534 (2018) 113–119.
[26] M. Ijaz Khan, Sohail A. Khan, T. Hayat, M. Imran Khan, A. Alsaedi, Electro-magneto flow of nanomaterial with irreversibility, Doi: https://doi.org/10.1016/j.cmpb.2019.105255.
[27] M. Beneš, I. Pažanin, Homogenization of degenerate coupled transport processes in porous media with memory terms, Math. Methods Appl. Sci. 42 (18) (2019) 6227–6258.
[28] E. Marušić-Paloka, I. Pažanin, M. Radulović, On the Darcy-Brinkman-Boussinesq flow in a thin channel with irregularities, Transp. Porous Media 131 (2020) 633–660.
[29] I. Pažanin, M. Radulović, Effects of the viscous dissipation on the Darcy-Brinkman flow: rigorous derivation of the higher-order asymptotic model, Appl. Math. Comput. 386 (125479) (2020) 1–12.
[30] R. Hamilton, O. Crosser, Thermal conductivity of heterogeneous two-component systems, Ind. Eng. Chem. Fundam. 1 (3) (1962) 187–191.
[31] Liu Yang, Xu. Xinyi, A renovated Hamilton-Crosser model for the effective thermal conductivity of CNTs nanofluids, Int. Commun. Heat Mass Transfer 81 (2017) 42–50.
[32] L.Th. Benos, E.G. Karvelas, I.E. Sarris, A theoretical model for the magnetohydrodynamic natural convection of a CNT-water nanofluid incorporating a renovated Hamilton-Crosser model, Int. J. Heat Mass Transf. 135 (June 2019) 548–560.
[33] N.S. Akbar, A.W. Butt, Ferromagnetic effects for peristaltic flow of Cu–water nanofluid for different shapes of nanosize particles, Appl. Nanosci. 6 (2016) 379–385.
[34] M.K. Saranprabhu, K.S. Rajan, Enhancement of solid-phase thermal conductivity and specific heat of solar salt through addition of MWCNT: new observations and implications for thermal energy storage, Appl. Nanosci. 9 (2019) 2117–2126.
[35] W. Yu, U.S. Choi, The role of interfacial layers in the enhanced thermal conductivity of nanofluids: a renovated Maxwell model, Nanoparticle Res. 5 (2003) 167–171.
[36] M. Mustafa, J. Ahmad Khan, Numerical study of partial slip effects on MHD flow of nanofluids near a convectively heated stretchable rotating disk, J. Mol. Liq. doi: 10.1016/j.molliq.2017.03.087.
[37] T. Hayat, Sohail A. Khan, M. Ijaz Khan, A. Alsaedi, Theoretical investigation of Ree-Eyring nanofluid flow with entropy optimization and Arrhenius activation energy between two rotating disks, Comp. Meth. Program Biomed. 177 (2019) 57–68.